5-2010

Flow rate measurement in a high temperature, radioactive, and corrosive environment

Taleb Moazzeni
University of Nevada Las Vegas

FLOW RATE MEASUREMENT IN A HIGH TEMPERATURE, RADIOACTIVE, AND CORROSIVE ENVIRONMENT

by

Taleb Moazzeni

Bachelor of Science
Shiraz University, Iran
1999

Master of Science
Petroleum University of Technology, Iran
2005

A dissertation submitted in partial fulfillment
of the requirements for the

Doctor of Philosophy in Electrical Engineering
Department of Electrical and Computer Engineering
Howard R. Hughes College of Engineering

Graduate College
University of Nevada, Las Vegas
May 2010

UNIVERSITY OF NEVADA LAS VEGAS

THE GRADUATE COLLEGE

We recommend the dissertation prepared under our supervision by

Taleb Moazzeni

entitled

Flow Rate Measurement in a High Temperature, Radioactive, and Corrosive Environment

be accepted in partial fulfillment of the requirements for the degree of

Doctor of Philosophy in Electrical Engineering
Electrical and Computer Engineering

Yingtao Jinag, Committee Chair

Jian Ma, Committee Member

Biswajit Das, Committee Member

Mei Yang, Committee Member

Hui Zhao, Graduate Faculty Representative

Ronald Smith, Ph. D., Vice President for Research and Graduate Studies
and Dean of the Graduate College

May 2010

ABSTRACT

Flow Rate Measurement in a High Temperature, Radioactive, and Corrosive Environment

by

Taleb Moazzeni

Dr Yingtao Jiang, Examination Committee Chair
Associate Professor of Electrical Engineering
University of Nevada, Las Vegas

Accurate measurement of coolant flow rate is essential for determining the maximum power required by the nuclear plant operation and critical for monitoring its operation safety. However, no practical off-the-shelf flowmeter is available to satisfy all the pressing multidimensional operation requirements (i. e., high temperature, high irradiation, and high corrosion). This work thus deals with the development of a new flowmeter for nuclear power plant/reactor process-monitoring and real time analysis; this proposed flowmeter shall be able to continuously conduct robust measurements under extremely harsh environment with high irradiation, high pressure, high temperature and corrosive media. We investigate a transit-time based flow rate measurement which is used in such environment. The transit time of a thermal signal travels along with a liquid flow can be obtained using a cross correlation method. This transit-time-based flowmeter using thermocouples with grounded stainless steel shielding is by far the most robust and reliable solution to measure the flow rate in a harsh environment typically seen in a nuclear reactor. In practice, cross correlation calculation tends to produce flat peak plateau or multiple peaks, leading to a significant error in peak detection. To overcome this problem, in this work, an Auto-Adaptive Impulse Response Function estimation (AAIRF) technique is introduced and a significantly narrower peak is shown theoretically

and also verified experimentally. In addition, we show that more accurate results can be obtained if moving average filter based cross correlation function (MAFCCF) is combined with AAIRF. Also in this work, we investigate a few important practical problems related to negative delays and sampling frequencies of the data acquisition.

The second part of this work deals with the calibration of the developed flowmeter which was mentioned above. To commission the flowmeter, calibration process is applied by comparing the reading measurements with a standard flowmeter measurement. In this work, this process is performed in an in house developed water-based test apparatus with a developed transit-time based flowmeter based on the measurement and processing of correlated thermal signals. In this system, we have observed that the accuracy of the measured flow is restricted to the time response of the thermocouples. In addition, since the flow rate is inversely proportional to estimated time delay, high flow rates measurement like 5 gpm (gallon per minute) requires large transit-time span that can not be achieved from a limited physical system dimensions. These problems are investigated through this work.

In the final part of this work, as the ultrasonic flow measurement technologies including transit-time and Doppler effect technologies are usually used in harsh environments, we study these methods with intensive simulations.

ACKNOWLEDGMENT

It was a pleasure working with the faculty, staff, and students at the University of Nevada, Las Vegas, during my study in the PhD program. This work has been possible by assistance and support I was given to pursue my research and study interests, thanks in advance to the kindness and considerable helping provided by Yingtao Jiang, my long-time advisor and committee chair. Jian Ma also deserves a great deal of thanks for his fruitful contributions to technical problems in this project.

This dissertation research has been sponsored by a Department of Energy TRP grant.

TABLE OF CONTENTS

LIST OF TABLES

LIST OF FIGURES

CHAPTER 1

INTRODUCTION

The measurement of flow rates (mass flow rates or volume flow rate) is an essential activity in a variety of industries and utility services. It also plays a notable role in monitoring and controlling the experimental conditions. The bulk flow rates can be obtained through direct methods, which measure the amount of discharged fluids over a period of time. Alternatively, flow rates can also be obtained using in-direct methods. For example, they can be derived through the measurement of fluid velocities. There are many ways in which the flow of the fluid can be measured including [1]: differential pressure flowmeters (primary element options, pitot tubes, variable area flowmeters), mechanical flowmeters (positive displacement, turbine, and other rotary flowmeters), electronic flowmeters (magnetic, vortex, and ultrasonic flowmeters), and mass flowmeters (Coriolis mass, thermal mass flowmeters, and hot-wire anemometers).

So far the flow velocity has been found in strong correlation with signals of pressure, temperature, optical wave, and ultrasonic wave etc, based on diverse physical principles, [2], [3]. In the application of liquid metal coolant flow rate measurement, the high temperature, pressure, corrosion environment limits most flow meter devices from being used in long term and maintenance-free operation. In addition, due to the strong radiation, high temperature and pressure in such applications like in the reactor core of a nuclear power plant or in the reactor vessel, in general it is difficult to measure local flow. The temperature measurement technique which is based on correlated thermal signals is well developed for high temperature applications [4], [5]. In the following, the main limitations with conventional flowmeters are summarized.

1.1. Momentum Sensing Meters

One big class of flowmeters is based on momentum sensing that the flow rate or flow velocity is derived from the momentum equation of fluid dynamics. Variable area meter (tube and float meter), spring-loaded diaphragm meter, target meter are typical examples [6]. The force from direct contacted fluid exerts on the float, diaphragm, or target is related to the fluid flow rate. The straightforward operation of this type of sensor makes it popular in a lot of applications in industry. However, the drawback of direct-contact excludes this flowmeter from being applied to corrosive environments. The material degradation of float, spring or target will have adverse effect on flow rate measurement.

In general, any device (such as orifice) in a flow duct will generate pressure drop (or loss), the flow rate correspondent to the pressure loss can be derived from Bernoulli's equation (or momentum equation, generally speaking) [6]. That is, the flow rate can be obtained from the pressure change between two reference locations that have different cross-sectional areas. Typical flowmeters based on the principle described here include orifice plate meter, Venturi meter or Dall tube meter, averaging pitot, and wedge/ V cone design meter, etc.

As this kind of flowmeters relates flow rate measurement to direct pressure measurement using some pressure sensor(s), it is thus necessary to examine pressure sensors against high temperature, corrosion and irradiation environments. Unfortunately, the corrosion and high temperature environment will quickly lead to a deadly failure of common pressure transducers (resistance variation to tensor on a diaphragm). Irradiation is another impacting factor that can generate significant errors of resistance measurement, consequently on the pressure measurement.

Piezoelectric sensors can measure various physical quantities, with pressure and acceleration being the most common ones. If a piezeoelectric sensor is used to measure the pressure, a membrane and a massive base are needed to ensure that an applied pressure specifically loads the elements in one direction. The deformation of piezoelectric material by pressure exert on it can generate a detectable voltage signal that can be related to the applied pressure. Piezoelectric technology is insensitive to electromagnetic fields and radiation, enabling measurement under irradiation environments. However, the high temperature is a big barrier that a piezoelectric pressure sensor can not tolerate.

Although some piezoelectric materials (gallium phosphate or tourmaline) have shown high stability at high temperatures, which may be translated to sensor temperature tolerance up to 1000 °C [7], the working temperature range for pressure sensor based on piezoelectric technology is far below that level. In the open literature, we have found that one product, K-12 pressure sensor from Piezo technologies, can be used up to 593 °C continuously and up to 760 °C intermittently. The corrosion resistance of K-12 sensor is not available in the literature. If the installation, sealing of diaphragm and other engineering issues have to be considered, this K-12 sensor shall work below 593 °C.

Above discussions have clearly indicated that the various flow meters based on pressure measurements are not practical for the applications in the high temperature (typically above 600 °C) corrosive and radiation environment.

1.2. Vortex-shedding, Swirl, and Fluidic Flowmeters

Vortex flow meter is another big class of sensor to measure the flow rate, and it is based on the phenomenon of Karman-vortex-street, which shows close to linear relationship between vortex shedding frequency and Reynolds number for certain range

of Reynolds number. As such, the measurement of flow rate is transformed to the measurement of vortex frequency, which is normally achieved by using a pressure sensor. As described before, the high temperature is a barrier for this type of sensor to be applicable in nuclear industry. In addition, material degradation of blunt body inside a vortex flowmeter due to corrosion/erosion will also lead to significant measurement errors. Actually, the same corrosion/erosion problems will have negative impacts on orifice plate flowmeters.

1.3. Other Intrusive Flowmeters

Other intrusive flowmeters include turbine and related flowmeters (Pelton wheel flowmeters, vane-type flowmeters etc.), positive displacement flowmeters (Helical rotor meter, reciprocating piston meters, precision gear flowmeters etc.), angular momentum devices, Coriolis flowmeters, and hot-wire thermal flowmeters etc. Due to the material degradation caused by corrosion/erosion, large measurement error, or even a total failure of sensor, is inevitable during a long term operation in nuclear plant.

1.4. Non-intrusive Flowmeters

Non-intrusive technologies, such as electromagnetic flowmeter and ultrasonic flowmeter, have been considered to replace intrusive flow meters to overcome the corrosion/erosion problem at high temperature. Laser Doppler Anemometry has been recognized as a leading non-intrusive velocity measurement technology. However, this technology cannot be used in fluids where no light can pass through as is the case of liquid metal coolant. Another problem is that this technology requires the inclusion of tracking particles to reflect the optical Doppler signal [8]. But it is impractical to introduce those small tracking particles into a nuclear reactor system.

Ultrasonic flowmeter can be an alternative to overcome the shortcomings of optical anemometry when dealing with an opaque fluid. The ultrasonic applications actually became really attractive until the development of piezoelectric transducers [9]. In general, there are a few different types of ultrasonic flowmeter, including the transit-time flowmeter, the Doppler meter and the cross-correlation flowmeter.

Similar to laser Doppler anemometry, an ultrasonic Doppler flow meter depends on the Doppler frequency shift, which occurs when sound wave bounces off a moving object. When most fluids flowing through pipelines are clean without any wave reflecting particles, this flowmeter may fail to measure the flow rate, as reported in [6].

Other ultrasonic flowmeters can be categorized as Wetted (transducer immersed directly to fluid) and non-wetted transducers. The wetted transducers for high temperature and corrosive environment encounter the same technical problems caused by high temperature as piezoelectric technology is used. The non-wetted transducer is protected by a metal window or even the pipe wall. However, it was noticed that there is a significant variation of ultrasonic wave propagation if wall roughness changes [10]. As a result, the ultrasonic flowmeter has to be frequently re-calibrated due to the inner surface degradation by corrosion/erosion.

Another non-intrusive flow rate measurement technology is electromagnetic flowmeter, which is based on Faradey's law of electromagnetic induction. The principle of this flowmeter limits its application for only conductive fluids. The very low voltage detected by flowmeter is a function of linear flow velocity, dimension of pipe (ID and OD), electric conductivities of the pipe wall, liquid and contact resistance at the liquid-

wall boundary. The variation of inner diameter, contact resistance due to long term corrosion/erosion will lead to considerable measurement errors [11].

This dissertation investigates the practical problems with the flow measurement technologies in the corrosive environments. The main contribution of this work which is directly related to the motivation of our research is to address the practical problems with a special flowmeter called correlated thermal signals based flowmeter.

Chapter two introduces the theoretical background behind this method and solutions to related problems with time delay estimation as it is the key point for calculation of flow rate in this method. In this chapter, we discuss the problems which we conducted in experiments with some signal processing solutions to overcome these problems.

Chapter 3 deals with the calibration procedures which is performed to derive the flow rate from the measured time delay. In this chapter, some related problems with calibration such as dependency of the flow measurement accuracy on the Reynolds number and physical settings are discussed.

Chapter 4 presents a theoretical study on the application of ultrasonic flow measurement technologies in corrosive environments. This chapter also provides a computer simulation on the main problem with this technology in such environment which is the pipe inner surface roughness.

Finally, chapter five gives some future direction issues for further study and research associated with this work.

CHAPTER 2

TIME DELAY ESTIMATION IN CORRELATED THERMAL SIGNALS

2.1. Introduction

In advanced nuclear reactors with a strong irritation, high pressure and temperature (>300 ^{o}C – 1000 ^{o}C), accurate measurement of coolant flow rate over an extended period of time is essential for safe operation [5]. Combination of irradiation, high temperature and high corrosiveness in a medium has imposed great challenges for flow rate measurement.

Many flow measurement technologies have been applied in various industries including momentum sensing meters (variable area meter [12], [13], spring-loaded diaphragm meter and target meter [14], [15]), vortex flowmeter, turbine and related flowmeters, positive displacement flowmeters, angular momentum devices, Coriolis flowmeters [16] and non-intrusive technologies, such as electromagnetic flowmeter and ultrasonic flowmeter [17]-[20]. Among all these flowmeters, only the non-intrusive ones are capable of working in corrosive environments.

The non-intrusive electromagnetic flow rate measurement technology is only good to be used in such harsh environment for a short time, as long term corrosion/erosion would change contact resistance at the liquid-wall boundary, leading to escalated measurement errors [15]. The ultrasonic flowmeters can be broadly categorized into wetted and non-wetted transducers, and they both suffer from corrosion problems. The wetted transducers are directly immersed in fluid and thus corrosive environment will gradually degrade the performance of the transducer. The non-wetted transducers demand frequent re-

calibration as the degradation of pipe inner surface caused by corrosion/erosion produces significant variation of ultrasonic wave [19].

This work thus deals with the development of a flowmeter to be used in a harsh environment such as a nuclear power plant/reactor for process-monitoring and real time analysis with reliable and accurate measurement. The transit-time of inherent random temperature fluctuations in processes, like the coolant flow in a nuclear reactor, can be obtained by the cross correlation calculation of flow temperatures recorded by two separate temperature sensors placed certain distance apart [20]-[23]. In specific, the first thermocouple placed at an upstream position on the flow senses a signature of temperature fluctuation, while the second downstream thermocouple ideally grabs the same signature with a delay that is inversely proportional to the flow rate. Determination of this delay through the cross correlation calculation of these two temperature signals will thus reveal the flow rate of interest.

Theoretically speaking, flowmeters based on this method can be employed in a harsh environment provided temperature sensors built upon corrosion- and radiation-resilient materials, like stainless steel with grounded shielding, are used. Practically, the cross correlation calculation that this scheme is based upon can generate a wide peak or a weak peak which may not be distinguishable from the one caused by background gamma radiation [5]. In either case, the accuracy of this technique is questionable. This problem, to some extent, is alleviated if the generalized cross correlation method [25] is used. However, this method requires *a priori* knowledge of the power spectra of both the signal and the noise, or it can give poor performance if the estimated spectra do not match well with the true spectra [26].

As an attempt to address the aforementioned problems in the cross correlation and the generalized cross correlation methods, one approach based on impulse response estimation using transfer function calculation was introduced in [15]. We tested this method experimentally using an in-house developed test apparatus, and results showed that this method unfortunately generates multiple peaks with same or similar height, leading to possible wrong readings.

As a result, in this work, we present an Auto-Adaptive Impulse Response Function estimation (AAIRF) technique, and we will theoretically show that a significantly narrower, stronger peak can be obtained, and this desirable property is also experimentally verified. The accuracy of AAIRF can be further improved if a proposed moving-average-filter-based cross correlation function (MAFCCF) is combined with AAIRF. Moreover, in this work, we will try to address a few important practical problems related to negative delays and sampling frequencies of the data acquisition. With all these techniques in place, one shall expect that a highly reliable sensor can be developed in a harsh environment that currently no other sensors can succeed.

The rest of this chapter is organized as follows. In section two, the time delay estimation methods including the cross correlation function, the transfer function estimation and the proposed methods are presented. In section three, the accuracy and error analysis of the proposed methods is given. Section four presents the test apparatus for the experiments and the experimental results are reported. Section five gives the results and discussions. Finally, section six concludes the chapter.

2.2. Time Delay Estimation Techniques

Assume that there is a negligibly small change in the characteristics of flow profiles, provided the thermocouples are within certain distances (Fig. 2.1). As a good rule of thumb, the thermocouples are spaced approximately three times of the pipe diameter [22], [24]. This promises high correlation between the downstream and the upstream signals. In order to generate the thermal signals that can well track the temperature fluctuation in a real setting, a heater that generates heat impulses can be employed.

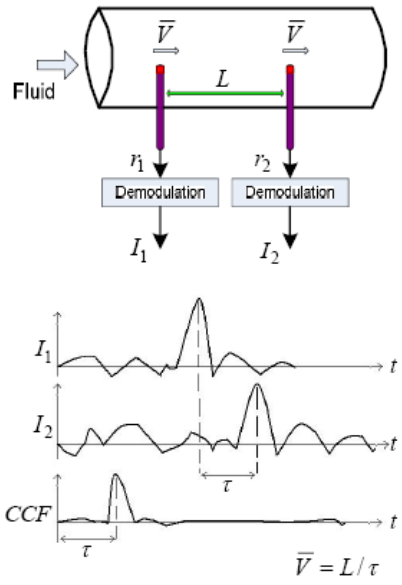

Fig. 2.1. Transit time configuration.

In this case, the upstream thermocouple records a flow signature $L/\overline{V}$ seconds earlier than the downstream one, where L is the distance between the two sensors and $\overline{V}$ is the average flow speed. By comparing the thermal signals obtained from the two thermocouples, we are able to determine the time delay, τ, thus the flow speed given as follows,

$$\overline{V} = L/\tau \tag{2.1}$$

The time delay can be traditionally obtained using two methods: the cross-correlation function-based and the transfer-function-based methods.

2.2.1. Cross-correlation Method

The principle behind this method is that the cross correlation calculation of the two correlated signals creates a peak which gives an indication of the time delay between the two thermocouples [15]. The cross correlation of $i_1(t)$ at time *t* and $i_2(t)$ at time $t-\theta$ is obtained from the average of the product of the two values over the observation time [22]. This method includes following major steps:

1) Calculate the cross correlation function (CCF) of the two thermocouple input signals $i_1(t)$ and $i_2(t)$.

$$CCF(\theta)=\int_{-\infty}^{+\infty} i_1(t)i_2(t-\theta)dt \tag{2.2}$$

where θ is the time delay between $i_1(t)$ and $i_2(t)$

2) Detect the peak of $CCF(\theta)$ to obtain τ. Since $i_2(t)$ is treated as a faithful copy of $i_1(t)$ delayed by τ, one has,

$$CCF(\theta)=\int i_1(t)i_2(t-\theta-\tau)dt = ACF(\theta-\tau) \tag{2.3}$$

where *ACF* is the autocorrelation function of $i_1(t)$.

Since the autocorrelation function (ACF) always has its maximum at time lag of zero, the cross correlation function (CCF) between these two signals, defined in Eq. (2.2), reaches its maximum after τ [15]. That is, the amount of time that CCF reaches its peak is actually the time delay of interest, τ. In a simple word, detection of maximum peak of CCF gives the time delay, τ.

2.2.2. Transfer Function Estimation Method

The first method which uses the maximum value of the CCF of the measured signals has two main problems: (i) the obtained peak is too wide which has negative impact on the result accuracy and (ii) besides the main peak which yields the expected time delay, there can be other undesirable peaks. To alleviate this problem, the transfer function estimation approach was recently proposed which tends to give a narrower peak to get the time delay [15]. Unlike the previous method, the system here is modeled as shown in Fig. 2.2. The measured signals $i_1(t)$ and $i_2(t)$ are considered as respective input and output of the model [15], and $h(t)$ is the impulse response function of the system.

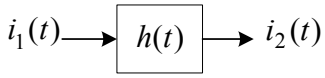

Fig. 2.2. System model for basic transfer function estimation.

It is shown that the CCF of $i_1(t)$ and $i_2(t)$ is equal to the impulse response function of the system, $h(t)$, provided that the applied signal at the first thermocouple is an impulse function, $i_1(t) = \delta(t)$ [15]. It means that the maximum peak of $h(t)$ corresponds to the time delay, τ, as the CCF does. Therefore, estimation of τ boils down to obtaining $h(t)$.

- *Practical estimation of the transfer function (TF):*

To obtain an unbiased estimation of the TF, it is supposed that the measured signals $i_1(t)$ and $i_2(t)$ have some added white noise. In this case, the system shown in Fig. 2.2 becomes the one shown in Fig. 2.3 [15]. The input and output of this model are

I_b and I_k, respectively, and W_1 and W_2 are the respective added noise to the input and the output. The transfer function, $H(j\omega)$, is obtained by [15],

$$\frac{CPSD_{12}}{APSD_1} = \frac{H}{1+\frac{|W_1|^2}{|I_b|^2}} \tag{2.4}$$

where $CPSD_{12}$ is the cross-power spectral density of I_1 and I_2, and $APSD_1$ is the auto power spectral density of I_1. In Eq. (2.4), since the $\frac{|W_1|^2}{|I_b|^2}$ is much less than 1, we may ignore this term to get the following expression of the estimated transfer function.

$$\hat{H} = \frac{CPSD_{12}}{APSD_1} \tag{2.5}$$

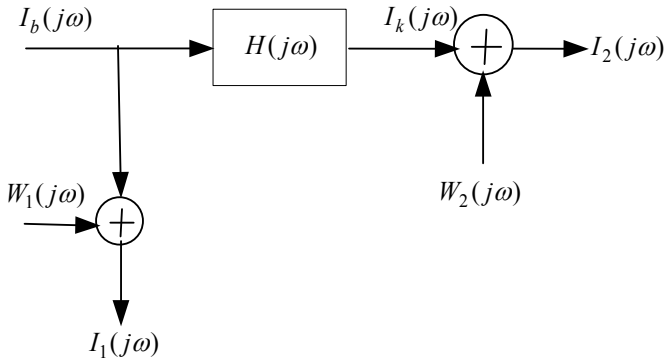

Fig. 2.3. Transfer function estimation with added white noise.

This algorithm includes following major steps:

1) Convert the time domain signals $ACF(t)$ and $CCF(t)$ to their frequency representations to get $APSD_1$ and $CPSD_{12}$, respectively.

2) Apply Eq. (2.5) to obtain $H(j\omega)$ and convert it back to $h(t)$ with inverse Fourier transform.

3) Detect the peak of $h(t)$ to obtain τ.

2.2.3. Auto-Adaptive Impulse Response Function Estimation Method

The conventional transfer estimation method using cross correlation and autocorrelation calculations mentioned in above section suffers from multiple peaks problem due to the fluctuations of the temperature in the coolant flow and additional fluctuations due to detection (statistical) uncertainties [15]. In Fig. 2.4, we show a result obtained from an experiment conducted in our lab using an in-house developed test apparatus. One can see that as the estimated impulse response function using the conventional transfer function is used, the actual delay point can hardly be detected from the multiple peaks. To alleviate this problem, a method called Auto-Adaptive Impulse Response Function estimation (AAIRF) is proposed. In this method, for transfer function and thus impulse function estimation, windowed cross correlation and autocorrelation functions are used. To do so, only the region around the peak that is detected by the cross correlation method is taken into account, and such a region can be chosen between two adjacent valley points around the peak.

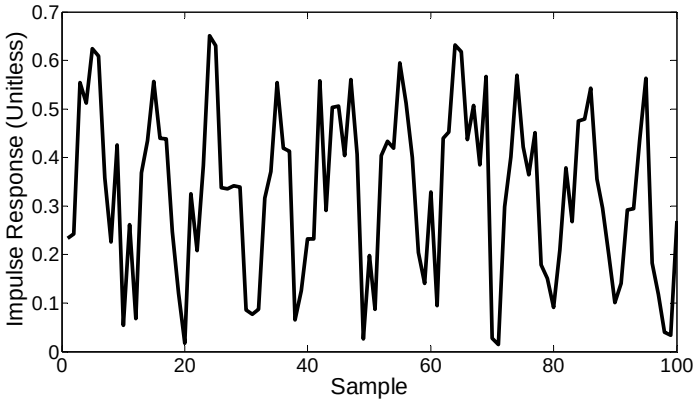

Fig. 2.4. Some impulse response of the system obtained from conventional transfer function estimation.

Assume that $ACF(t)$ and $CCF(t)$ have multiple peaks as shown in Figs. 2.5.a and 2.5.b. Let $\psi_{11}(t)$ and $\psi_{12}(t)$ be the respective windowed functions of $ACF(t)$ and $CCF(t)$ (Figs. 2.6.a and 2.6.b). $\psi_{12}(t)$ can be expressed in terms of $\psi_{11}(t)$ as follows,

$$\psi_{12}(t) = \psi_{11}(t-\tau) + \delta\psi_{11}(t-\tau) \tag{2.6}$$

Let $\widetilde{H}(j\omega)$ be the Fourier transform of the system based on the windowed correlation function. By transforming Eq. (2.6) to frequency domain via Fourier transform, one may find,

$$\begin{aligned}
\widetilde{H}(j\omega) &= \frac{F\left(\psi_{12}(t)\right)}{F\left(\psi_{11}(t)\right)} = \frac{F\left(\psi_{11}(t-\tau) + \delta\psi_{11}(t-\tau)\right)}{F\left(\psi_{11}\right)} \\
&= \frac{\Psi_{11}(j\omega)}{\Psi_{11}(j\omega)} e^{-j\omega\tau} + \frac{\Delta\Psi_{11}(j\omega)}{\Psi_{11}(j\omega)} e^{-j\omega\tau} = \left(1 + \frac{\Delta\Psi_{11}(j\omega)}{\Psi_{11}(j\omega)}\right) e^{-j\omega\tau} \\
&= \left(1 + \left|\frac{\Delta\Psi_{11}(j\omega)}{\Psi_{11}(j\omega)}\right| e^{j(\phi_{\Delta\Psi_{11}} - \phi_{\Psi_{11}})}\right) e^{-j\omega\tau}
\end{aligned} \tag{2.7}$$

Since $\psi_{11}(t-\tau)$ and $\delta\psi_{11}(t-\tau)$ are in close phase and the amplitude of $\delta\psi_{11}(t)$ is much smaller than that of $\psi_{11}(t)$, Eq. (2.7) yields following approximation for $\widetilde{H}(j\omega)$,

$$\widetilde{H}(j\omega) \cong e^{-j\omega\tau} \tag{2.8}$$

Therefore,

$$\widetilde{h}(t) \cong \delta(t-\tau) \tag{2.9}$$

Eq. (2.9) indicates that the obtained impulse response function $\widetilde{h}(t)$ is theoretically close to an impulse function, and thus it shall have one single extremely narrow and strong peak at point τ .

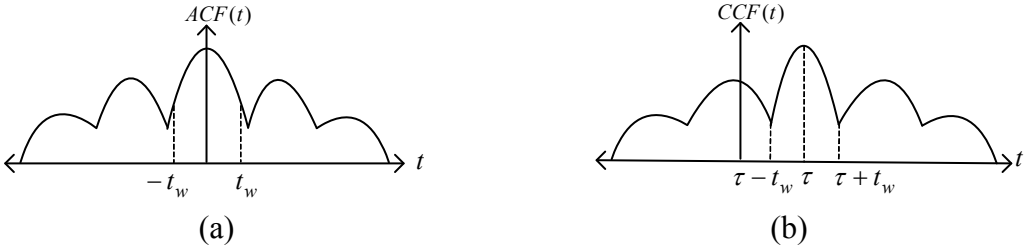

Fig. 2.5. (a): The autocorrelation function of $i_1(t)$, (b): The cross correlation function of $i_1(t)$ and $i_2(t)$.

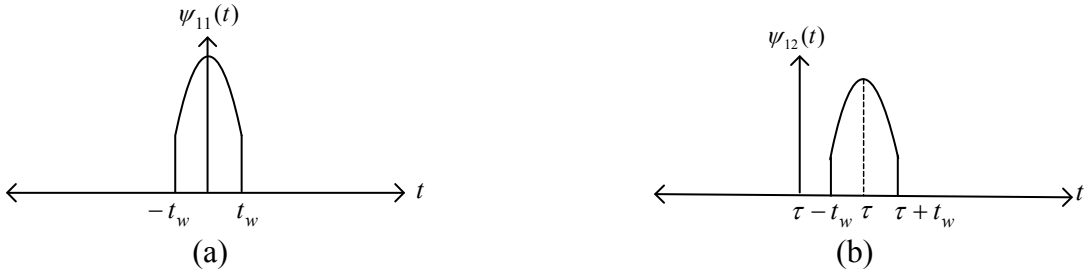

Fig. 2.6. (a): The windowed version of the autocorrelation function of $i_1(t)$, (b): The windowed version of cross correlation function of $i_1(t)$ and $i_2(t)$.

2.2.4. Moving Average Filter based Cross correlation Function method

Although the Auto-Adaptive Impulse Response Function estimation method gives a very narrow and strong peak, the considered window and thus the accuracy of detected peak is dependent on the peak point deviation in cross correlation function. In other words, deviation of the cross correlation estimate affects the performance of this method. To alleviate this problem, we employ another method called Moving Average Filter based Cross Correlation Function (MAFCCF) [27]. In this method, the raw data are simply averaged over some interval, followed by cross correlation calculation using the filtered data. This MAFCCF function can be expressed as,

$$R_{i_1 i_2}(rT_s) = \frac{1}{T}\sum_{k=1}^{N-1} i_{1M}(kT_s) i_{2M}((k-r)T_s) \tag{2.10}$$

where

$$i_{1M}(kT_s) = \frac{1}{M}\sum_{l=0}^{M-1} i_1((k-l)T_s) \tag{2.11}$$

$$i_{2M}((k-r)T_s) = \frac{1}{M}\sum_{l=0}^{M-1} i_1((k-r-l)T_s) \tag{2.12}$$

where r is the number of sampled-data in CCF, k is the number of sampled-data in signals $i_1(t)$ and $i_2(t)$, T_s is the sampling period, and M is the length of moving average filter.

2.3. Accuracy and Error Analysis

The accuracy of the cross correlation time delay detector depends on the measurement of the peak value of the cross correlation function. The major sources of errors include the bandwidth of measured signals, number of samples, background noise, waveform sampling, waveform quantization and distortion of the trace pattern in the flow

between the thermocouples (and TC responses) [28]. In addition, there are several possible sources of systematic error, such as filter mismatch, pipe diameter variations and differences between the geometrical and effective thermocouple spacing [28]. In this study, we found the system error is negligibly small as compared to the error due to time delay estimation method and the sampling frequency.

2.3.1. Error due to time delay estimation method (cross-correlation function)

It can be shown that the respective normalized mean square error in cross correlation function and the variance of time delay estimates τ_* are given by [28]:

$$e^2(\tau)=\frac{1}{2BT}\left[1+\frac{1}{\rho^2 xy(\tau)}\left(1+\frac{1-q}{f_s T}\right)^2\right] \tag{2.13}$$

$$\mathrm{var}(\tau^*)=\frac{0.038}{TB^3}\left\{\left[\frac{1}{\rho^2 xy(\tau^*)}\left(1+\frac{1-q}{f_s T}\right)^2\right]-1\right\} \tag{2.14}$$

$$\rho^2 xy(\tau)=\frac{CCF^2(\tau)}{ACF_1(0)ACF_2(0)} \tag{2.15}$$

where B is the bandwidth of measured signals, T is the length of measured signals, ACF_1 and ACF_2 are the respective autocorrelation functions of $i_1(t)$ and the cross correlation of $i_1(t)$ and $i_2(t)$, f_s is the sampling frequency, $\rho^2{}_{xy}(\tau)$ is the normalized cross correlation, and q is the correlation coefficient between the instantaneous flow event. This correlation coefficient for the measured signals can be obtained by [28]:

$$q=1-\frac{f_s T}{SNR} \tag{2.16}$$

where SNR is the mean square signal to noise ratio that may be estimated from the measured normalized cross correlation by [28]:

$$SNR = \frac{\rho^2{}_{xy}(\tau)}{1-\rho_{xy}(\tau)} \tag{2.17}$$

As the *SNR* in MACCF is larger than that in CCF, according to Eqs. (2.16) and (2.13), the normalized mean square error of time delay estimates in MACCF will be smaller than that in CCF method.

2.3.2. Error due to the sampling frequency

As we use ADC and DAC devices, the sampled-data form is used in calculations. Thus, the cross correlation function is calculated point by point as shown in Fig. 2.7. This function gives the position of peak, not the real time delay. The time delay is obtained by dividing the detected number where the peak occurred by the sampling frequency (Fig. 2.7). If the sampling frequency is not large enough, it may make an error in the calculation of the time delay as shown below.

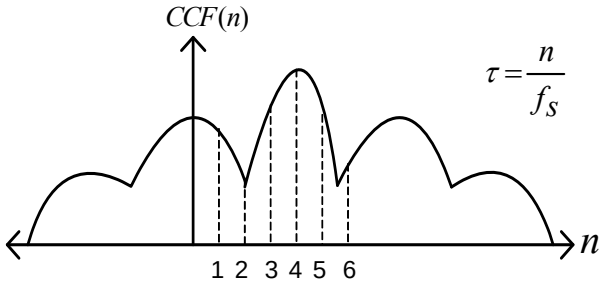

Fig. 2.7. Point by point cross correlation.

The flow rate is related to the time delay between the two thermal signals as follows,

$$Q = VA = \frac{L}{\tau}\frac{\pi D^2}{4} \tag{2.18}$$

where Q is the flow rate, V is the flow velocity, A is the cross-sectional area of the pipe, L is the distance between two thermocouples, τ is the time delay between the two thermal signals, and D is the internal diameter of pipe.

Substituting $\tau = \frac{\theta}{f_s}$, where θ is the sample offset delay between two thermal signals, into Eq. (2.18) gives,

$$Q = \frac{K}{\tau} = K\frac{f_s}{\theta} \tag{2.19}$$

Taking derivative with respect to f_s yields,

$$\frac{\Delta\tau}{\Delta f_s} = -\frac{\theta}{{f_s}^2} \tag{2.20}$$

Combining Eq. (2.19) and (2.20) gives,

$$\frac{\Delta\tau}{\Delta f_s} = -\frac{K}{Qf_s} \tag{2.21}$$

By combining $\frac{\Delta Q}{\Delta\tau} = -\frac{K}{\tau^2}$ and Eqs. (2.19) and (2.21), one may get,

$$\frac{\Delta Q}{\Delta f_s} = \frac{Q}{f_s} \tag{2.22}$$

According to the above equation, the measured flow rate deviation with respect to the sampling frequency is dependent on the sampling frequency itself which can come with a larger error at a low sampling frequency.

2.3.3. Determination of the effective Bandwidth of the System

The bandwidth of the turbulent flow noise is usually wide; however, the thermocouples used in the system can filter out the high frequency components of the measured signals [29]. One approach to measure the bandwidth of the system was

introduced in [29] which is again based on the cross correlation calculations. Assume that the downstream signal, $i_2(t)$, can be approximated by letting the upstream impulse signal, $i_1(t)$, pass through a low pass filter and then get delayed by τ (Fig. 2.8). Then the normalized cross correlation function is given by [29]:

$$h'(t) = i_1(t) * i_2(t) = \sin(2\pi B(t-\tau))/2\pi B(t-\tau) \tag{2.23}$$

As the bandwidth of the system (Fig. 2.9) with its impulse response given in Eq. (2.23) can be calculated by [29]:

$$B = \frac{1}{4\gamma} Hz \tag{2.24}$$

where γ is the deviation time from the peak point that takes the correlation function to reach $2/\pi$ of its maximum value.

Therefore, finding the system bandwidth boils down to determine the value of γ such that $h'(t \pm \gamma) = 2/\pi$.

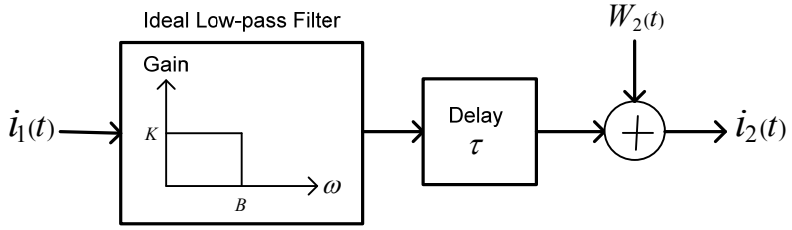

Fig. 2.8. Approximation to system model.

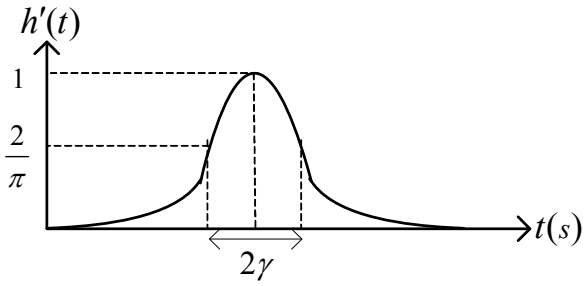

Fig. 2.9. Effective bandwidth representation of cross correlation function.

For instance, we found from one of experiments (Fig. 2.10) that γ is about 0.5 seconds. Correspondingly, the measured effective bandwidth of the system will be 0.5 Hz.

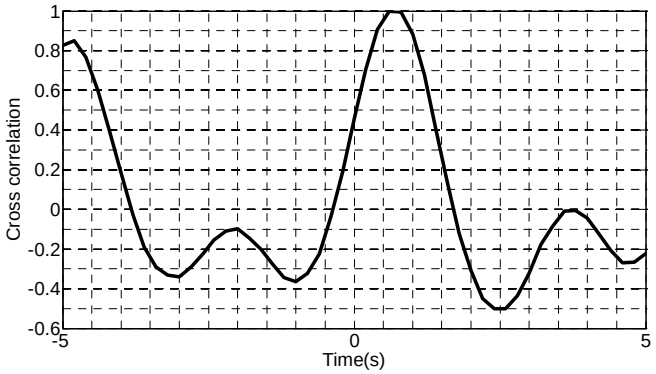

Fig. 2.10. Cross correlation of measured signals.

2.3.4.. Threshold Signal to Noise Ratio

The minimum signal to noise ratio (*SNR*) required to detect the peak point in the cross correlation function algorithm is achieved by [30]:

$$SNR_{Th} = \omega_0^{\,2} / B^3 T \tag{2.25}$$

where ω_0 is the center frequency of recorded signals, B and T are given in Eq. (2.24) and (2.13), respectively.

2.4. Eexperiments

To experimentally verify the proposed methods, we performed an experiment using a water-based test apparatus developed at our laboratory (Fig. 2.11). This system comprises of two thermocouples along the pipe, a water tank, a water pump for circulating the flow, an electrical heater for exciting the system and a data acquisition system for collecting the data and transferring them to a PC. The internal diameter of the pipe is 20.9 mm and the distance between the two thermocouples is 500.0 mm. This distance is so chosen so that it is three times longer than that of the pipe diameter (for reasons mentioned in section two). This way, the meter is able to measure wider time delay span with more accurate flow rate readings. In this experiment, the thermocouples have found to have the time constant of 1.4 seconds. The tips of the thermocouples are placed at the center of pipe. The data acquisition system uses the delta-sigma ADC with a resolution of 24 bits, maximum sampling rate of 475 KS/s and input bandwidth (-3 dB) of 15 Hz. As the system deals with a flow with a flow rate ranging from 0.5 gallon per minute (gpm) to 5 *gpm*, the corresponding Reynolds number is between 1.04×10^4 and 10.40×10^4 which means the flow is turbulent (Re>2300) [31].

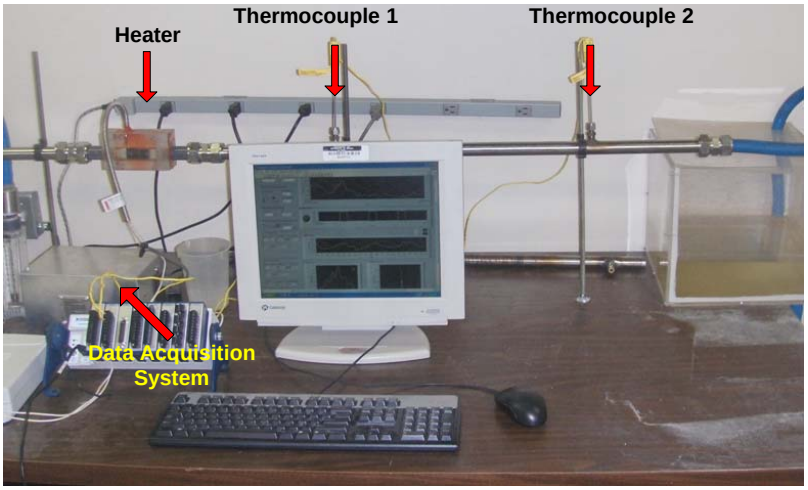

Fig. 2.11. A water-based test apparatus.

Experimental data obtained from this test apparatus are used for evaluation of different methods, CCF, AAIRF, and MAFCCF. The data are recorded in different flow rate levels ranging from 0.5 to 5 gpm with different heating patterns: periodic and random heating.

2.4.1 Experiments using Periodic Heating

To create a strong thermal signal in the system, the water flow in the test apparatus is periodically heated using the heater shown in Fig. 2.11. In order to evaluate how the period and the duty cycle of the heating signal may affect the accuracy of the time delay estimation, we have tested four different heating patterns as summarized in Table 2.1. Here flow rate is fixed to 0.5 gpm, sampling window size is set to 400, and the sampling frequency is 10 Hz.

Table 2.1. Periodic heating (heating pulse) patterns.

Heating Pattern	On Heating Time (s)	Off Heating Time (s)	Duty Cycle	Period (s)
1	1	4	20%	5
2	2	3	40%	5
3	1	7	12.5%	8
4	2	6	25%	8

2.4.2 Experiments using Random Heating: Sampling Window Size

In the second set of experiments, the heater shown in Fig. 2.11 is turned on/off in a random fashion to create temperature fluctuations in the water flow. Here we try to evaluate how the sampling window size may affect the accuracy of the time delay estimation. In these experiments, the sampling frequency is fixed to 10 Hz, but we vary the numbers of samples from 1 to 400 samples.

2.4.3 Experiments using Random Heating: Sampling Frequency

In the third set of experiments, we try to evaluate how the sampling frequency may affect the accuracy of the time delay estimation. Here again the heater is turned on/off in a random fashion to create temperature fluctuations in the water flow. In these experiments, the number of samples is fixed to 400 samples, and the sampling frequency sweeps from 1 to 40 Hz. Since the maximum response time of the thermocouples is 1.4 seconds, the minimum sampling frequency has to be chosen to satisfy the Nyquist sampling theorem, which is 0.23 Hz.

2.5. Results and Discussions

2.5.1. *Experiments using Periodic Heating*

In this set of experiments, we have found that if the period of the heating signal is not sufficiently higher than the time delay between the two thermal signals, the cross

correlation function tends to generate multiple peaks with same height and/or negative peaks. For instance, with the experiment setting mentioned in section 2.4.1, the estimated time delay is 4.2 seconds, when heating patterns 1 and 2 (Table 2.1) are applied with a period of 5 seconds, the side-lobe peaks are found to have the same height as the supposedly main peak. However, when heating patterns 3 and 4 are applied with a period of 8 seconds, about the twice of the time delay, these problems are gone.

Of all the four heating patterns (Table 2.1), it has been found that the duty cycle has no noticeable effect on the time delay estimation.

2.5.2. Effects of Sampling Window Size

The size of the sampling window has significant impacts on the accuracy of the time delay estimation. In the second set of experiments (section 2.4.2), we have examined the number of samples vs. variance of estimated time delay by using several methods, including CCF, the baseline AAIRF, and the proposed MAFCCF with its moving average filter assuming different lengths (i.e., 2, 4, and 6). That is, there are a total of five configurations, and their results are plotted in Fig. 2.12.

Both CCF and the baseline AAIRF methods give nearly identical variance of estimated time delay. But when the moving average filter is used, one can see from Fig. 1.12 that the variance is reduced, indicating improved accuracy. It can be found that the longer of the moving average filter, the less of the variance of estimated time delay.

For the same configuration in Fig. 2.12, one can see that when the size of the sampling window is below 270 samples, significant variance exists. When the size of the sampling window exceeds 270 samples, the accuracy improvement in terms of reduced variance of estimated time delay is very statistically small. When the sample size is near

400 samples, the variance is largely due to the system errors, and no improvement can be expected if the sampling window size goes higher. Therefore, in practice, the sampling window size is set to 400 samples for most of our experiments using the test apparatus shown in Fig. 2.11.

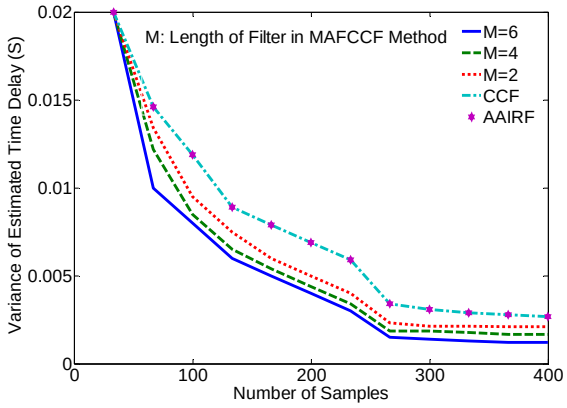

Fig. 2.12. Variance of estimated time delay for considered methods for flow rate of 2 gpm, sampling frequency of 10 Hz and for five different configurations: (i) CCF, (ii) AAIRF, (iii) MAFCCF with its moving average filter assuming a length of 2, (iv) MAFCCF with its moving average filter assuming a length of 4, and (v) MAFCCF with its moving average filter assuming a length of 6.

2.5.3. Effects of Sampling Frequency

Fig. 2.13 shows that the results of the sampling frequency (Hz) vs. deviation of calculated flow rate (gpm), which agrees well with the theoretical predications by Eq. (2.22). For all three flow rates in Fig. 2.13, when the sampling frequency is below 10 Hz, significant deviation has been observed, which corresponds to lower accuracy. Although we showed in section 2.4.3, that the minimum sampling frequency can be as low as 0.23 Hz, in practice, the sampling frequency has to be chosen higher to get reasonably low

deviation of the flow rate. When the sampling frequency exceeds 10 Hz, no significant reduction of the deviation of flow rate can be achieved. Therefore, in practice, the sampling frequency is set to 10 Hz for most of our experiments using the test apparatus shown in Fig. 2.11.

When the same sampling frequency (10 Hz) is used, we try to compare the accuracy of different methods, including CCF, the baseline AAIF, and the MAFCCF with its moving average filter assuming a length of 6. The results are reported in Table 2.2. Here two figures of merit are used: (i) the variance of time delay estimates, which is given in Eq. (2.14), and (ii) the Full Width at Half Maximum (FWHM), defined as peak height divided by its width (Fig. 2.14). In addition, these three methods are compared for their respective computation efficiency given in CPU time.

From Table 2.2, it can be seen that in terms of FWHM, the AAIF has much more accurate result than the other two at a higher computation cost. It is also seen that although the baseline AAIF method gives a very narrow peak to detect the peak point, its deviation of estimated time delay is the same as that of CCF method (Fig. 2.12), as AAIF and CCF both are based on the same correlation calculation. MAFCCF on the other hand, gives lower deviation of estimated time delay than AAIF and CCF.

Also from Table 2.2, for the same variance of estimated time delay of 0.005 seconds, the CCF and AAIF methods require longer CPU time than MAFCCF method. This means that the MAFCCF method requires fewer samples to converge to a given level of accuracy. As a result, when both accuracy and CPU time are concerned, the MAFCCF has its advantages over the other methods.

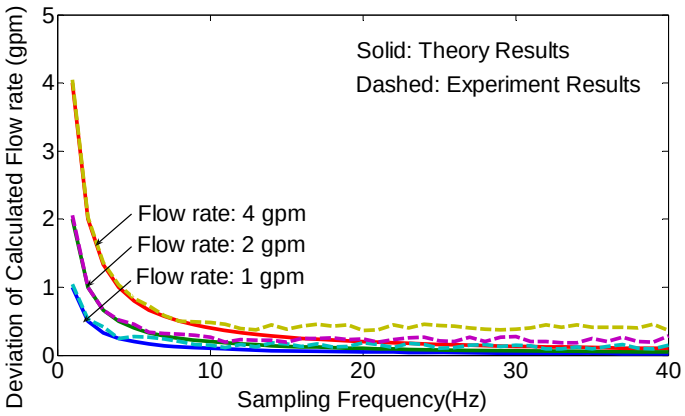

Fig. 2.13. Calculated flow rate deviation with respect to sampling frequency.

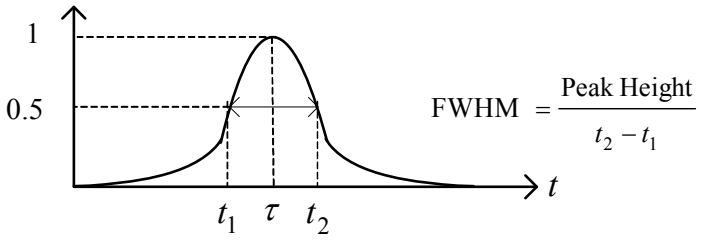

Fig. 2.14. The full width at half maximum representation.

Table 2.2. FWHM and CPU time comparison of the methods with the same variance of estimated time delay of 0.005 seconds.

Methods	FWHM	Normalized CPU Time
CCF	0.035	1
AAIF	1.653	1.12
MAFCCF (M=6)	0.042	0.45

2.6. Conclusions

Experiments indicated that for flow rate measurement in a harsh environment, the conventional methods that are based on the calculation of cross correlation function or transfer function suffer from a few signal processing problems; often undesirable wide peaks, and catastrophic negative or false peaks which may fail these methods will be generated. To address these problems, two methods, (i) the baseline AAIF and (ii) MAFCCF, were proposed in this paper, and they were experimentally verified. The results showed that the proposed baseline AAIF approach gives very narrow and sharp peak. When AAIF is combined with a moving average filter, this MAFCCF algorithm showed a few distinct advantages: (i) it generates extremely narrow peaks as AAIF does, (ii) it has the lowest normalized standard error than any other approaches, and (iii) it has low computation requirement suitable for real time processing.

CHAPTER 3

CALIBRATION

3.1. Introduction

There has been a growing demand world-wide for flow meter verification testing and calibration services [31]. Calibration is a set of operations and services that under specified conditions, establish the relationship between values of quantities indicated by a flowmeter and the corresponding values realized by standards [33]. In these operations, by measuring the error of indication of the meter, the output value from the meter has to be adjusted is corrected. The flowmeter is manufactured with a pulse output signal that is often marked with a correction coefficient called *K*-factor. The correctness of this factor is found out only after calibration [34]. Due to normal variation of *K*-factor with the flow, the meter needs to be calibrated at different flows for better accuracy [34]. The state of the art in the field of the liquid flow calibration is still being represented by a theoretical foundation dating back about 40 years [35].

There are two basic types of flowmeter calibration systems: primary and secondary systems [32],[36]-[38]. Primary systems uses fundamental measurements of mass, length (or volume), and time. In this case, a primary calibration is performed by measuring the volume or mass of the liquid moved over an elapsed time and compute the flow rate directly [39]. Examples include gravimetric (weigh tank) systems; bell-type provers; piston-type (swept volume) provers; and pressure, volume, temperature, and time systems (PVT) [32]. Secondary systems are those calibrated based on a primary system. These systems typically include experimentally determined calibration coefficients that take into account modeling simplifications.

Secondary calibration involves comparing the device to another, more accurate, device (i.e. another flow meter). However the second device must also be calibrated somehow, perhaps with a third, even more accurate device, but at some point we will run out of increasingly accurate measuring devices, and we will have to calibrate our reference device some other way, preferably by measuring the quantity of interest using more direct and simplified means [39]. Examples of secondary flow standards include turbine meters and critical flow Venturi (sonic nozzle) meters. To calibrate the flowmeter, the measurement uncertainty is the upper limit of the measurement error and often the most important issue that must be taken in account [39]. This error may have different sources so that based on the type of flowmeter, liquid and application, different calibration methods and calibration equipment are required for best results [40]. Furthermore, for each application, a particular flowmeter type may have different measurement uncertainty. As presented in [41], the uncertainty of the differential pressure flow meter type that used for a feed water flowmeter is 1.76%, while this error is reduced by replacing this flow meter with an ultrasonic flow meter having an uncertainty of 0.25% [42]. To reduce the measurement uncertainty, a new calibration facility was presented in Japan [43]. At these calibration facilities, the calibration of the feed water flow meter in the nuclear power plant has been discussed in order to carry out an uprate of thermal output (Okamoto and Kikura [43], [44]).

Based on the existing calibration procedures, one may found out that depending on the flow measurement method these processes are performed in different way. One common calibration strategy which is utilized in the cross correlation flow meters is curve fitting which uses extrapolation approach [45]. In this work, this approach is

developed in a cross correlation flowmeter based on the measurement and processing of correlated thermal signals. As a water-based test apparatus at the lab was constructed, the calibration results are verified by experiments. In this flow measurement system, we observed that the accuracy of the measured flow is restricted to the time response of the thermocouples. In addition, measuring higher flow rates like 5 gpm (gallon per minute) requires a larger transit-time span that can not be achieved from a limited physical system dimensions. These problems are investigated through this calibration work.

This chapter is organized as follows. In section two the flow velocity profile and flow rate calculation are discussed. In section three the flow rate range and resolution are presented. Section four introduces calibration factor estimation. Section five presents the experiments. Section six gives the results and discussions. Finally, section seven draws the conclusions.

3.2. Flow Velocity Profile and Flow Rate Calculation

In turbulent flow as we deal with it in this work, far away from the pipe wall, the flow is free from the friction that is the velocity is maximum. On the wall, the flow moves at the same velocity as the wall or $V = 0$. For turbulent flow an approximate curve-fit is given by [6],

$$\frac{V(r)}{\overline{V}} = \frac{(n+1)(2n+1)}{2n^2}(1-2r/D)^{1/n} \tag{3.1}$$

where $V(r)$ is the flow velocity at radial position *r*, *D* is the pipe diameter, $\overline{V}$ is the mean velocity , and *n* is a constant number which is related to the Reynolds number. In our work, for the corresponding Reynolds number which is between 1.04×10^4 and 1.04×10^5, *n* is equal to 6.6.

To obtain the flow velocity profile in our flow measurement system, we measured the velocity at several radial positions for flow rate range between 0.5 and 4 gpm. Using these data, an experimental equation is derived for the mean velocity which is given in section 3.6.

To derive flow rate from the velocity, the following equation is applied,

$$Q = K\overline{V}A \tag{3.2}$$

where Q is the flow rate, K is the calibration factor, $\overline{V}$ is the mean velocity, and A is the cross section of the pipe.

3.3. Flow Rate Range and Resolution

The time response of the thermocouples is one of limitations in the transit-time based flow measurement system. In this experiment, the thermocouples have found to have the time constant of 1.4 seconds. We observed that by sampling frequency above 10 Hz, the thermocouples give repetitive data. Therefore we fixed the sampling frequency to 10 Hz.

To derive the flow rate from the estimated time delay between thermal signals, the following equation is applied,

$$Q = VA = \frac{L}{\tau}\frac{\pi D^2}{4} \tag{3.3}$$

where Q and A are given in Eq. (3.2), V is the flow velocity, L is the distance between two thermocouples, τ is the time delay between the two thermal signals, and D is the internal diameter of the pipe.

For this system, using physical setting of $D = 0.02087\,m$ and $L = 0.5\,m$,

$$Q = \frac{1.71\times10^{-4}}{\tau}(m^3/s) \tag{3.4}$$

Since the cross correlation function is calculated in sampled-data format, the highest flow rate is achieved when the detected peak point is one. As the sampling frequency is 10 Hz, the corresponding time delay to this peak point is 0.1 second. Therefore,

$$Q_{\max} = \frac{1.71\times10^{-4}}{\tau_{\min}} = 1.71\times10^{-3}\, m^3/s = 27.11\, gpm$$

$$1 m^3/s = 15850.32\, gpm$$

If the detected peak point in the time delay estimation method deviates from a number to the adjacent number, the deviated flow will be,

$$\Delta Q = Q(n) - Q(n-1) = \frac{\pi D^2 L f_s}{4}\left(\frac{1}{n} - \frac{1}{n-1}\right) \tag{3.5}$$

where f_s is the sampling frequency and n is the sample offset delay between two thermal signals.

Using the calculation given in Eq. (3.4),

$$\Delta Q = Q(n) - Q(n-1) = 27.11\left(\frac{1}{n} - \frac{1}{n-1}\right) = -\frac{Q^2}{27.11 - Q} \tag{3.6}$$

Table 3.1 shows some numerical results for the resolution of the calculated flow versus flow range.

Table 3.1. Resolution of the calculated flow versus flow range.

Q (gpm)	0.5	1	1.5	2	2.5	3	3.5	4
ΔQ (gpm)	0.0094	0.0383	0.0879	0.1593	0.2540	0.3733	0.5188	0.6923

In general, Eq. (3.6) is expressed as,

$$\Delta Q = -\frac{4Q^2}{\pi D^2 L f_s - 4Q} \tag{3.7}$$

Figs 3.1 and 3.2 show some numerical results for the resolution of the calculated flow versus flow range for different settings of the thermocouple spacing and the pipe diameter.

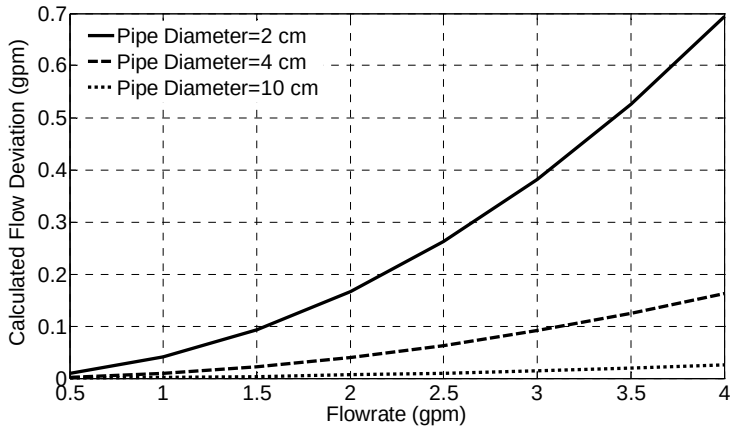

Fig. 3.1. Resolution of the calculated flow versus flow range for different pipe diameters and thermocouple spacing of 0.5 m.

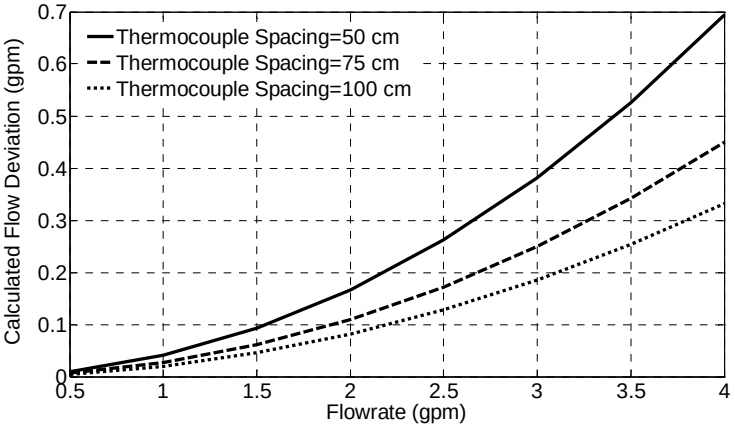

Fig. 3.2. Resolution of the calculated flow versus flow range for different thermocouple spacing and pipe diameter of 2 cm.

3.4. Calibration Factor Estimation

As seen in the Eq. (3.3) the calculated flow is sensitive to the pipe geometry and the thermocouple spacing. However, since the measured flow is based on the temperature fluctuations which makes a very small change in the temperature profile, these quantities can be assumed to be fixed. Moreover, since the roughness of the wall paper does not affect the temperature profile, therefore the calibration factor is not sensitive to this factor. Therefore the only factor that is taken in account for calibration factor estimation is the measurement error due to either the background noise or the time delay estimation techniques errors. To minimize this error two fitting models are examined.

3.4.1. Linear Fitting

The simplest way to estimate the calibration factor is to apply linear fitting. In this case, the calculating formula for instantaneous flow Q is [46],

$$Q_C = KQ_m \tag{3.5}$$

where Q_C and Q_m is the calibrated and measured flow rate, respectively, and K is the calibration factor which is obtained through calibration procedure.

The optimum value of the unknown parameter K is obtained by minimizing the sum of the square errors as [47],

$$e^2 = \frac{1}{N}\sum_{n=1}^{N}\left(Q_r(n) - KQ_m(n)\right)^2 \tag{3.6}$$

where N is the number of calibration point, Q_r is the reference flow rate which is read form the standard flowmeter, and $Q_m(k)$ is the measured flow rate.

By taking the derivative of error equation with respect to K and setting the obtained equation to zero, the calibration factor is achieved. That is,

$$\hat{K} = \frac{\sum_{n=1}^{N} Q_r(n)}{\sum_{n=1}^{N} Q_m(n)} \tag{3.7}$$

3.4.2. Non-linear Fitting

Based on several realizations, it was observed that the measured flow is not linearly proportional to the reference flow. This suggests to apply the polynomial curve fitting as follows,

$$Q_c = k_p Q_m{}^{P} + k_{p-1} Q_m{}^{P-1} + \ldots + k_0 \tag{3.8}$$

where k_i are coefficients to be estimated .

3.5. Experiments

Experimental data obtained from the test apparatus was used for estimation of calibration factor. To do so, firstly, some experiments were performed to find the flow velocity profile and the best redial poison for placing the thermocouple tips. Here, the thermocouples are placed at different radius point from 0 (the pipe center) to 0.8 (close to the pipe wall), the sampling window size is set to 400 and the sampling frequency is 10 Hz. Figs. 3-5 show the flow velocity profile for the reference flow of 0.5 to 4 gpm.

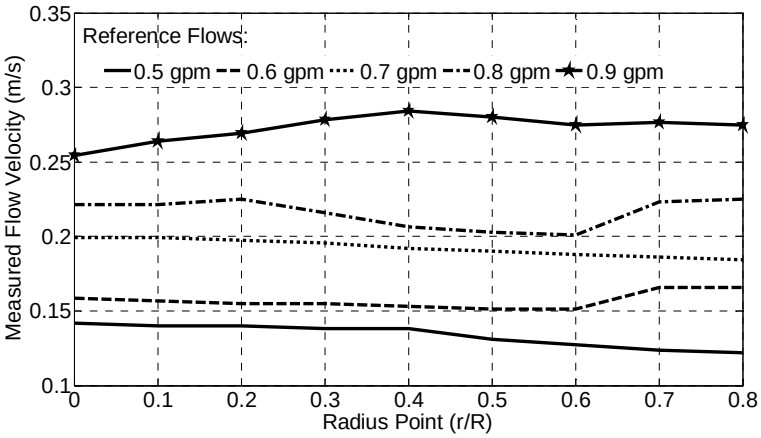

Fig. 3.3. Flow velocity versus radius point

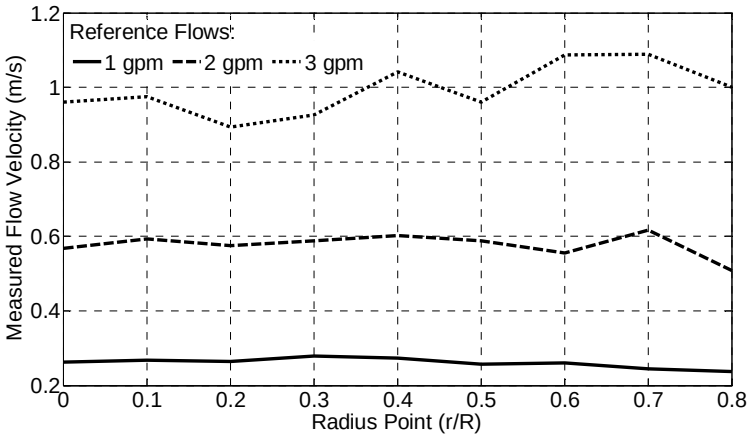

Fig. 3.4. Flow velocity versus radius point

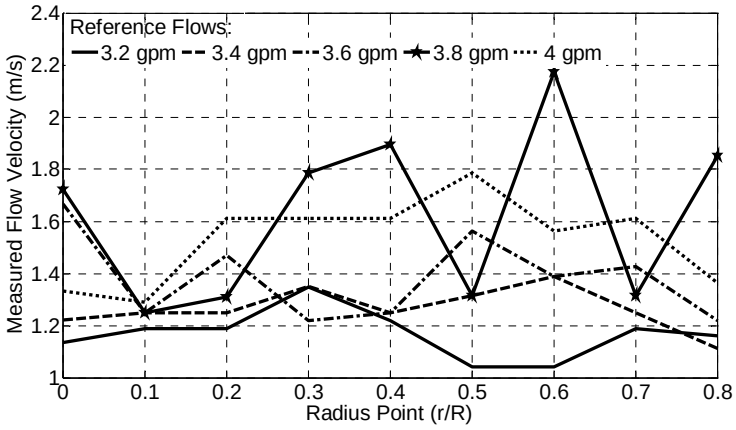

Fig. 3.5. Flow velocity versus radius point

3.6. Results and Discussions

To choose the best location of the thermocouples tips across the pipe, two considerations are taken in account: (i) the normalized mean square error of measured transit-times and (ii) the relationship between the measured flow velocities at each location with the mean flow velocity. From the Table 3.2, it is seen that the normalized mean square errors for radius points less than 0.7 are likely the same. Therefore, from the accuracy point of view any location interior this radial position can be chosen for the thermocouple tips location. Also, from the Figs. 3.3-3.5, it is seen that the flow velocity over radius interval point [0, 0.3] are not changed much so that the mean velocity over this interval is close to the velocity measured at each point. That is,

$$V(r) \cong \overline{V} \qquad 0 \le r \le 0.3R \tag{3.9}$$

Therefore, any location interior this radial position gives easy calculation for measurement.

Table 3.2. The normalized mean square error of measured transit-times versus radius point

Flowrate (gpm)	0	0.2	0.3	0.4	0.5	0.6	0.7	0.8
1.0	0.0029	0.0029	0.0035	0.0037	0.0027	0.0034	0.0044	0.0032
2.0	0.0035	0.0035	0.0045	0.0038	0.0040	0.0043	0.0056	0.0064
2.8	0.0152	0.0145	0.0173	0.0198	0.0128	0.0167	0.0267	0.0367
3.9	0.0189	0.0194	0.0230	0.0213	0.0313	0.0278	0.0898	0.0691

The first calibration factor estimation was done by applying linear fitting method. As shown in Table 3.3, the calibration factor is increased with the flow rate which implies that the measured flow rate is not linearly proportional to the actual flow rate. The other calibration experiment is to apply a polynomial function to the measured data. Tables 3.4 and 3.5 show the results for the polynomial of order 2 and 3, respectively. It shows that the second order approximation gives more accurate results. To test the repeatability of

the measurements and results, we use 3 sets of experimental data which recorded in 3 different times. As shown in Fig. 3.6, the fitting curve remains nearly the same for each set of measurement which means that the fitted curves is able to extrapolate the experimental data.

Another investigation of calibration test is the dependency of the flow rate on the Reynolds number, as the flow is turbulent. Here, the calibration factor is expressed in terms of the Reynolds number. According to equation $\mathrm{Re} = \frac{\rho V d}{\mu}$, where V is the flow velocity, for this system we have, $\mathrm{Re} = 1.04\times10^{4} V = 1.04\times10^{4}\frac{L}{\tau} = 0.57\times10^{4}\frac{1}{\tau}$. Using Eq. (3.5) and measurement results for the second polynomial fitting, one may get,

$$CF = \frac{Q_m}{Q_a} = 10^{-4}\left(1.8425(\mathrm{Re})^2 + 1.2784(\mathrm{Re}) + 3.5309\right) \tag{3.10}$$

where CF is calibration factor, Q_m and Q_a are the measured and the reference flow rate, respectively. The results for the second order model are shown in Figs. 3.6 -3.8.

Table 3.3. Ratio of the measured flow to reference flow

Reference Flow (gpm)	Measured Flow (gpm)	Ratio of the Measured Flow to the Reference Flow
1.06	1.3735	1.3735
2.02	3.0229	1.5114
2.85	4.5487	1.5116
3.92	6.9423	1.7358

Table 3.4. Second order polynomial fitting results

Experiments	k_2	k_1	k_0	MSE
1	0.4142	0.0524	1.1294	0.0321
2	0.3874	0.2688	0.7424	0.0319
3	0.4033	0.1019	1.0817	0.0331

Table 3.5. Third order polynomial fitting results

Experiments	k_3	k_2	k_1	k_0	MSE
1	0.0133	0.3073	0.3590	0.7771	0.0354
2	0.0062	0.3484	0.3134	0.7867	0.0430
3	0.0241	0.2268	0.4892	0.7691	0.0482

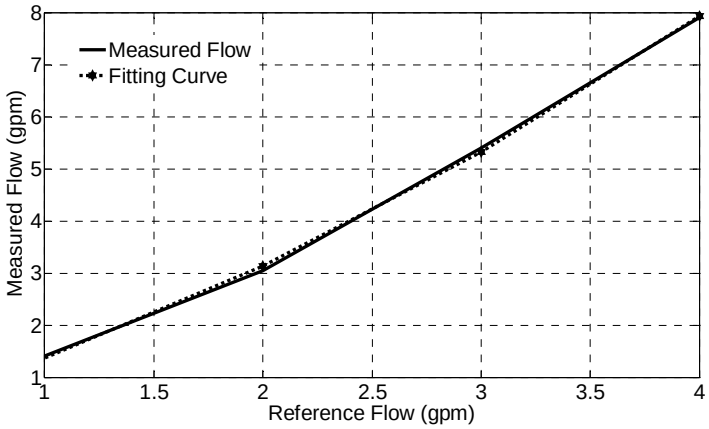

Fig. 3.6. Second order polynomial fitting

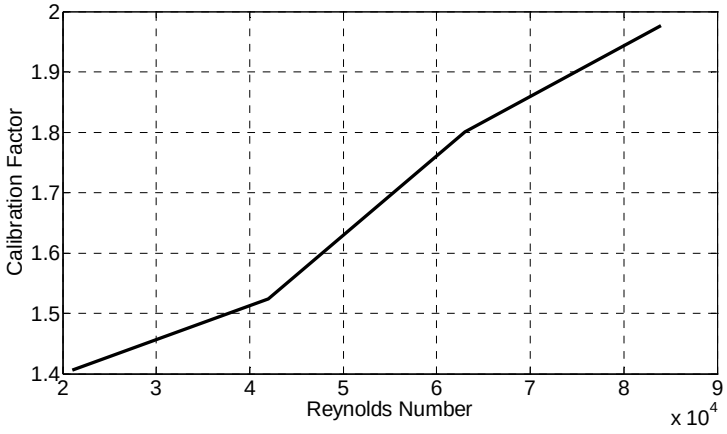

Fig. 3.7. Calibration curve

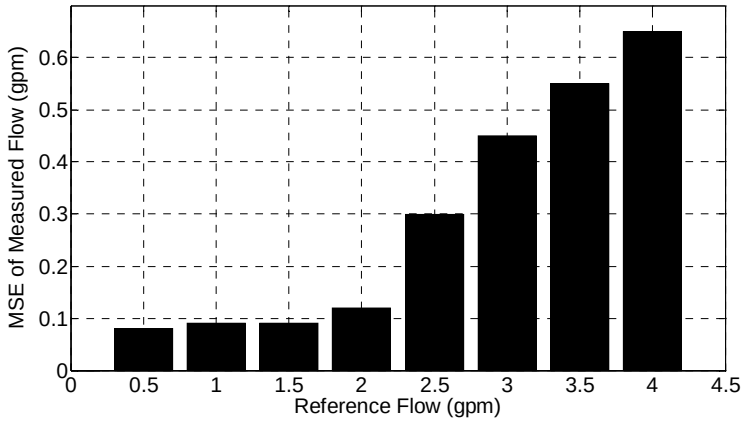

Fig. 3.8. Mean square error of measured flow

3.7. Conclusions

A polynomial model of calibration for cross correlation flowmeter was developed which predicts the output of the flowmeter based on the estimated transit-time of correlated thermal signals. The model was verified using experimental data recorded in the lab calibration facility. The dependency of the calibration factor on the Reynolds number and the flow range were expressed. While experimental data for limited Reynolds number were used for the calibration, the model may provide a basis for a procedure to extrapolate lab measurements to the higher Reynolds numbers in realistic applications.

CHAPTER 4

ULTRASONIC FLOWMETERS

In this chapter, firstly, a brief background of ultrasonic flowmeters is given. Next, a theoretical study with computer simulations on the effect of the pipe surface roughness on the accuracy of the ultrasonic flow measurements is presented.

4.1. Theoretical Background

Ultrasonic flowmeters works in general with two different principles: (i) Doppler effect ultrasonic flowmeter and (ii) transit time ultrasonic flowmeter. A brief description of these flowmeters are given as follows,

4.1.1. Doppler Effect Ultrasonic Flowmeter

In this technology, an ultrasonic beam is transmitted to the flow. When this beam is reflected by suspended particles or gas bubbles in flow, its frequency is shifted. This shift in frequency is proportional to the flow velocity as follows [48],

$$v = c(f_r - f_t)/2f_t \cos\phi \tag{4.1}$$

where f_r is received frequency, f_t is transmitted frequency, v is flow velocity, ϕ is the angle between the transmitted beam and the flow axis, and c is the sound velocity in the flow. Fig. 4.1 shows a schematic of this flowmeter.

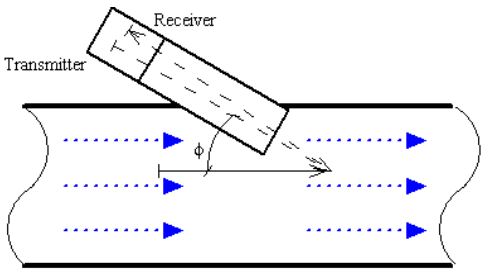

Fig. 4.1. A schematic of the Doppler effect ultrasonic flowmeter.

This method requires some reflecting particles such as gas bubbles or solid particles to act as scatterers of ultrasound beam in the flow [48].

- *Advantages of the Doppler Effect Ultrasonic Flowmeter* [49]-[51]

Doppler meters may be used in such environments that other meters are not capable of working such as raw sewage, sludge, slurries, paper pulp, tar, sands, and oil-water-gas mixtures slurries and aerated liquids. The main advantages can be summarized to:

- can be mounted outside the pipes
- has less obstruction with flow
- has low flow cut off
- can be used in corrosive environment
- relatively consumes low power

- *Limitations of Doppler Effect Ultrasonic Flowmeters* [48]

The major limitations in the Doppler flowmeters are the nature, size, and spatial of the particles or bubbles in the flow which are required for scattering. This leads to variation and attenuation of the ultrasonic beam. The flowmeter senses the velocity of the scatters and due to slippage it might not correspond to the flow velocity. Also, the relationship between the scatter velocity and the mean flow velocity is unknown. Furthermore, any disturbance, bends, valves, pipe work and probes may cause vortices which can make error in reading [48]. Also, the measurement is sensitive to the physical properties of flow, sound, and scatterers such as the conductivity of the sound, the density of reflectors, the temperature of flow, and the flow profile. If the particles in the pipe are not uniformly distributed in the pipe cross section, it may result in error in flow reading. These problems limit Doppler flowmeter in highly accurate measurement applications.

4.1.2. Transit-time Ultrasonic Flowmeter

In this technology, two transducers transmit and receive signal sounds between the two transducers and measure the transit-time between the two transducers (Fig. 4.2). The difference in the downstream and upstream transit-times is directly proportional to the flow velocity as shown in the following,

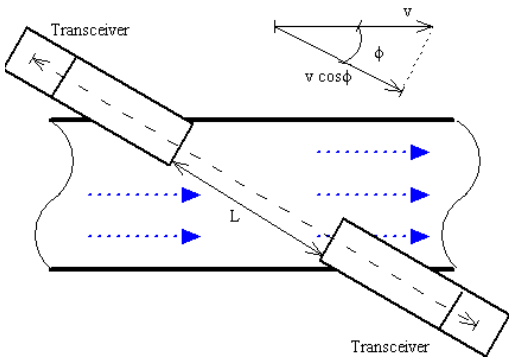

Fig. 4.2. A schematic of the transit-time ultrasonic flowmeter.

$$t_d = L/(c + v\cos\phi) \tag{4.2}$$

$$t_u = L/(c - v\cos\phi) \tag{4.3}$$

where t_d is the downstream transit-time, t_u is the upstream transit-time, L is the distance between transducers, c is the sound velocity, and ϕ is the angle between the transmitted beam and the flow axis.

By combining Eq. (4.2) and (4.3) and considering $c >> v$, one may get,

$$t = t_d - t_u = 2vL\cos\phi/(c^2 - v^2\cos^2\phi) = 2vL\cos\phi/c^2 \tag{4.4}$$

- *Advantages of Transit-time Ultrasonic Flowmeters over Doppler Flowmeter* [48]

▪ no need reflector particles inside the pipe.

▪ unaffected by the size and density of any particle inside the pipe

- *Advantages of Doppler Flowmeter over Transit-time Flowmeters* [50]

▪ less sensitivity to the internal surface roughness of the pipe

▪ less sensitivity to Reynolds number

▪ uninfluenced by the velocity profile across the pipe

▪ capable of directly measuring instantaneous flow velocities

4.2. A Review of Experimental Works

This section summarizes a few experimental works which have been presented in the following literatures,

A. [49]:

This work concentrated on realization of flow velocity profile for measurements of liquid metal lead–bismuth eutectic (LBE), flow velocity profile in the spallation neutron source target model by the ultrasonic Doppler flowmeter. It reports that either wetting property of LBE with stainless steels or performance of supersonic probes at high temperatures is poor. To enhance the intensity of reflected ultrasonic wave, the surface treatment of LBE container was examined. It was found that the solder coating was effective.

B. [50]:

In this work the Doppler ultrasonic flowmeter is applied at hydraulic power stations. It mentions that the ultrasonic the Doppler flow meters are suitable tools to measure flow rates in steel penstocks. This work reports that the transit-time ultrasonic flowmeters require a meter factor which is heavily influenced by the velocity profile across the pipe. Occasionally, after the recalibration of an ultrasonic flowmeter a shift of the calibration factor has been observed [51]. The suspected cause of this shift is the sensitivity of the ultrasonic flow meter to flow profile changes [52]. The flow profile depends on the internal pipe wall roughness which can be affected over time by wear, pitting, corrosion, or internal contamination [10]. In contrast, the ultrasonic Doppler flowmeter does not require this kind of correction factor. Here, the transducer is installed on the outside surface of the pipe, (Figs 4.3 and 4.4).

In order to obtain sufficiently strong ultrasonic echoes, some important parameters in selecting a Ultrasonic flowmeter are the pipe size, wall thickness and flow velocity. For large piping, the Nyquist constraint balancing between maximum measurable depth and maximum measurable velocity becomes very challenging. Table 4.1 illustrates the typical ultrasonic setting in this field test.

Table 4.1. Ultrasonic setting in the field test

Ultrasonic Parameters	Value
Basic Frequency	400-500 kHz
Pulse repetition frequency	300-500 Hz
Cycle per Pulse	8-12 waves/pulse
Chanel distance	10-15 mm
Sampling interval per profile	250-500 ms
Number of data points per profile	128
Number pulse repetitions	128
Transducer driving voltage	30 Vp-p

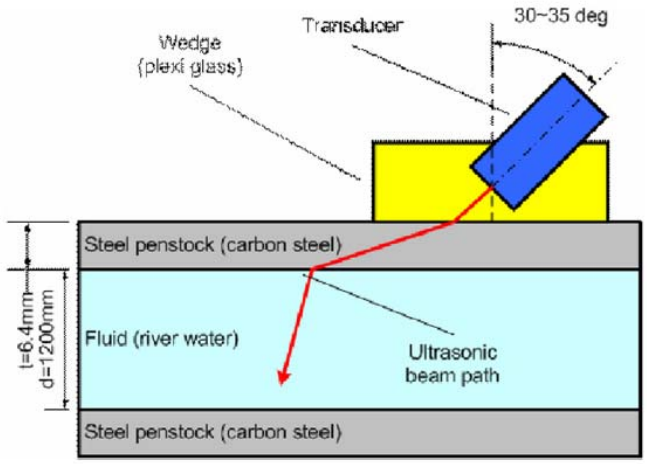

Fig. 4.3. Schematic diagram of the ultrasonic transducer installed on the pipe surface.

Fig. 4.4. Ultrasonic transducer and wedge which are installed on the outside surface of the pipe.

C. [53]

In this work the fabrication, evaluation and several applications of high performance clad metallic buffer rods for ultrasonic transducer at elevated temperatures is developed. Some applications with high temperature operating ranges are reported, e.g. $7008^{o}C$ for aluminum (Al) die casting [53], 200–$4008^{o}C$ for polymer extrusion [10], and $15008^{o}C$ for molten glass [54] and steel [52]. The performance of high temperature piezoelectric ultrasonic such as lithium niobate, and particularly that of the couplant, is inadequate above approximately $4008^{o}C$. Therefore, the ultrasonic transducer with buffer rods is preferable for process monitoring at high temperatures. In this approach, one probing end of the buffer rod is in contact with the material, and the other end can be cooled by water or air.

D. [55]:

In this work, the clamp-on transit-time and cross-flow-type ultrasonic flowmeters, which are strapped onto the outside of a pipe, are introduced to nuclear power plants. It is

reported that these methods require flow profile factors determining the theoretical velocity profiles, and strongly depend on the real flow profiles. As these factors are affected by turbulent flows and inner surface wear in the pipe under aging phenomena, a new flow metering system in a circular pipe, an ultrasonic velocity profile method has been developed [54], [56]. In this method, the instantaneous velocity profiles across the pipe is directly measured, next, the flow rate is calculated using the integration over space of the averaging velocity profiles [57], [58].

4.3. Effects of Surface Roughness on Clamp-On Ultrasonic Flowmeters

In corrosive environments such as nuclear power plants, clamp-on ultrasonic flowmeters which are not in touch with the flow can be applied [57]-[60]. These meters are available in two formats: transit time and Doppler. Both technologies feature clamp on designs based on the transducer which detect flow rates from outside the pipe. As power plants age significantly, the readings of flowmeters in reactor feed water systems drift due to the changing flow profile [59]. The flow profile depends on the internal pipe wall roughness which can be affected over time by wear, pitting, corrosion, or internal contamination [61]. Pipe surface roughness is a major contributor to the flow profile which changes unpredictably from smooth to rough Therefore, the measurement accuracy of ultrasonic flowmeters which in the sound wave incident to the internal surface pipe is sometimes questionable in the large high-pressure, high-temperature piping in actual power plants [59].

As shown in Fig. 4.5, when measuring the transit-time between upstream and downstream ultrasonic signals, the ultrasonic beam deflection deviated by the internal pipe wall roughness which is called carry-along (sound drift) effect. This leads to two

problems: (i) in the case of high beam deviation, excessive bending of the beam path causes the beams to miss the opposing transducer and (ii) as reported in [54], deviation of ultrasonic incidence angles and radiation angles shown in Fig. 6 have a significant impact on flow measurement accuracy. When using the Doppler ultrasonic meter, although the first problem is not revealed, as seen in Fig. 4.5 the reflected beam may not reach the transducer in case of large pipe surface roughness.

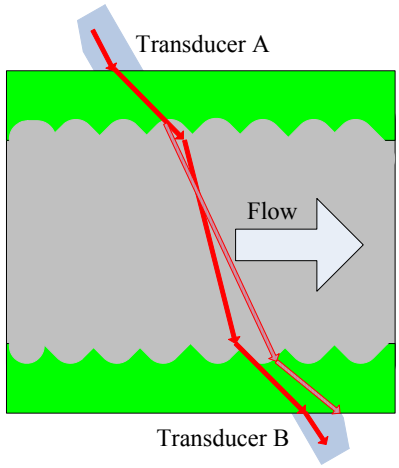

Fig. 4.5. Ultrasonic beam sound paths through the pipe: the solid path is for the smooth surface and the dashed path is for the rough surface.

The effect of pipe surface roughness on ultrasonic meter performance has been studied in a few literatures [62]-[66]. However, the problem formulation for the effect of wall changes on ultrasonic meters was not available. In this work, to investigate the influence of surface roughness, a theoretical model relevant to the effect of pipe surface roughness on the velocity profile calculated by transit-time as well as Doppler ultrasonic flowmeter is presented.

4.3.1. Transit-time Ultrasonic Flowmeter

In the corrosive application, on the interior surface that is exposed to the flow an oxidized layer is formed. For simplification, we consider one equivalent layer composed of oxidized and wall so that only two interfaces between media are used in the analysis. For the smooth interface, the ultrasonic beam travels in a route as shown in Fig 4.6. In this case, we have,

$$\frac{\sin\alpha_t}{\sin\alpha_w} = \frac{C_t}{C_w} \tag{4.5}$$

$$\frac{\sin\alpha_w}{\sin\alpha_f} = \frac{C_w}{C_f} \tag{4.6}$$

where α_t is the angle of incidence in the transducer, α_w is the angle of refraction in the pipe wall, α_f is the angle of incidence in the flow, C_t, C_w, and C_f are the speed of sound in the transducer, pipe wall and flow, respectively.

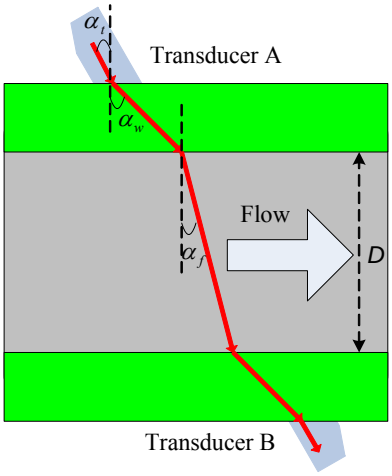

Fig. 4.6. Ultrasonic beam path through pipe with smooth surface.

To consider the effect of corrosion on the interface between the pipe wall and the flow, as an irregularly striped pattern may form on the pipe's inner surface, there is not

any deterministic or even a special random pattern to model this roughness. One simple assumption is to model the roughness pattern by a uniform distribution described as follows,

$$h_1 = k_1 \sin\theta_1 \tag{4.7}$$

$$h_2 = k_2 \sin\theta_2 \tag{4.8}$$

where k_1 and k_2 are deterministic parameters and θ_1 and θ_2 are independent random variables with probability density functions of,

$$f(\theta_1) = f(\theta_2) = \begin{cases} \dfrac{1}{\pi} & -\dfrac{\pi}{2} < \theta < \dfrac{\pi}{2} \\ 0 & Otherwise \end{cases} \tag{4.9}$$

where $h_{\max}$ is the maximum level of the surface roughness.

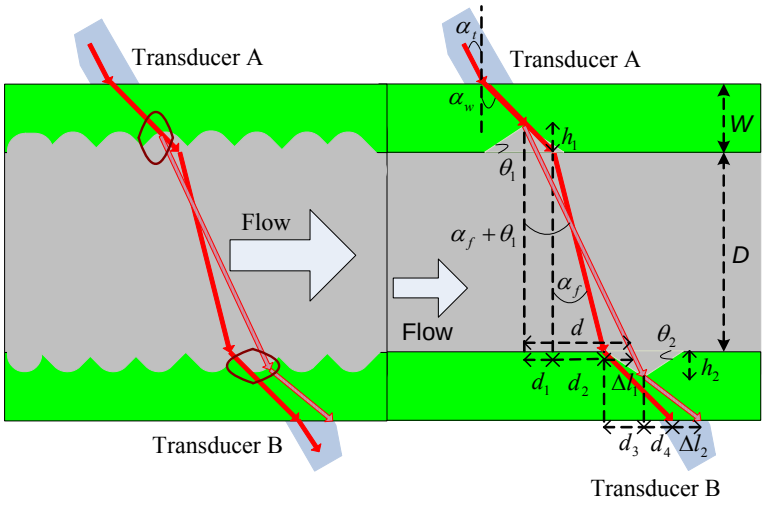

Fig. 4.7. Ultrasonic beam sound paths through the pipe: the solid path is for the smooth surface and the dashed path is for the rough surface.

For the above pipe side, one may have,

$$d_1 = h_1 \tan(\alpha_w) \tag{4.10}$$

$$d_2 = D\tan(\alpha_f) \tag{4.11}$$

$$d = (D + h_1)\tan(\alpha_f + \theta_1) \tag{4.12}$$

Using Snell law,

$$\alpha_w = Arc\sin\left(\frac{C_w}{C_t}\sin(\alpha_t)\right) \tag{4.13}$$

$$\alpha_f = Arc\sin\left(\frac{C_f}{C_t}\sin(\alpha_t)\right) \tag{4.14}$$

Therefore,

$$\Delta l_1 = d - d_1 - d_2 = (D + h_1)\tan(\alpha_f + \theta_1) - D\tan(\alpha_f) - h_2\tan(\alpha_w) \tag{4.15}$$

For the bellow side of pipe, one may have,

$$\frac{\sin(\alpha_f + \theta_1 + \theta_2)}{\sin(\alpha_{w2})} = \frac{C_f}{C_w} \tag{4.16}$$

where α_{w2} is the angle of refraction in the pipe wall in case of rough surface.

$$d_4 + \Delta l_2 = (W - h_2)\tan(\alpha_{w2} - \theta_2) \tag{4.17}$$

$$d_4 + d_3 = W\tan(\alpha_w) \tag{4.18}$$

$$d_3 = h_2\cot(\theta_2) \tag{4.19}$$

Therefore,

$$\Delta l_2 = (W - h_2)\tan\left(Arc\sin\left(\frac{C_w}{C_f}\sin(\alpha_f + \theta_1 + \theta_2)\right) - \theta_2\right) - W\tan(\alpha_w) + h_2\cot(\theta_2) \tag{4.20}$$

- Calculation of maximum acceptable roughness level

If the deviation of ultrasonic beams is large, the opposite transducer may not sense the transmitted beam. To find the maximum acceptable roughness level such that the

deviated beams are received by the opposite transducer, we should have, $\Delta l \le (\Delta l_1) + (\Delta l_2)$.

Since θ_1 , θ_2, h_1, and h_2 are random variables, the obtained beam drifts Δl_1 and Δl_2 will be also random variables. To find the total beam drift that is the sum of random variables Δl_1 and Δl_2, a statistical analysis is done which is presented in Appendices A and B.

- *Calculation of the flow velocity error due to deviation of ultrasound beams*

For the smooth surface pipe the the respective downstream and upstream transit times T_{down} and T_{up}, and the flow speed V_S are given by,

$$T_{down} = \frac{D}{\sin\gamma(C_f + V_S\cos\gamma)} \tag{4.21}$$

$$T_{up} = \frac{D}{\sin\gamma(C_f - V_S\cos\gamma)} \tag{4.22}$$

$$V_S = \frac{D(T_{up} - T_{down})}{T_{up}T_{down}\sin 2\gamma} \tag{4.23}$$

where γ is the angle between downstream beam and the flow axis.

In the rough surface pipe, as seen in Fig 4.7, the ultrasound beams are bended. In this case, the respective downstream and upstream beams get deviated by θ_1 and θ_2 which are resulted in changing γ to $\gamma+\theta_1$ and $\gamma+\theta_2$. Therefore, the respective downstream and upstream transit times, and the flow speed are changed to,

$$\left(T_{down}\right)_R = \frac{D}{\sin(\gamma-\theta_1)\left(C_f + V_S\cos(\gamma-\theta_1)\right)} \tag{4.24}$$

$$\left(T_{up}\right)_R = \frac{D}{\sin(\gamma-\theta_2)\left(C_f - V_S\cos(\gamma-\theta_2)\right)} \tag{3.25}$$

$$V_R = 2D\frac{\left(T_{up}\right)_R \sin(\gamma-\theta_2) - \left(T_{down}\right)_R \sin(\gamma-\theta_1)}{\left(T_{up}\right)_R\left(T_{down}\right)_R\left(\sin 2(\gamma-\theta_1)\sin(\gamma-\theta_2) + \sin 2(\gamma+\theta_2)\sin(\gamma-\theta_1)\right)} \qquad (3.26)$$

where $\left(T_{up}\right)_R$ and $\left(T_{down}\right)_R$ are the respective upstream and downstream transit-times in the rough surface pipe.

Therefore, the change in the flow speed will be,

$$\Delta V = V_R - V_S = D\left(2\frac{\left(T_{up}\right)_R \sin(\gamma-\theta_2) - \left(T_{down}\right)_R \sin(\gamma-\theta_1)}{\left(T_{up}\right)_R\left(T_{down}\right)_R\left(\sin 2(\gamma-\theta_1)\sin(\gamma-\theta_2) + \sin 2(\gamma-\theta_2)\sin(\gamma+\theta_1)\right)} - \frac{(T_{up}-T_{down})}{T_{up}T_{down}\sin 2\gamma}\right) \qquad (4.27)$$

To measure the difference between the smooth and rough pipe flow speeds, ΔV, as the change in the flow speed are due to two independent beam deviations θ_1 and θ_2, the root mean square error of ΔV can be described as,

$$RMSE(\Delta V) = \sqrt{\frac{(\Delta V_1)^2 + (\Delta V_2)^2}{2}} \qquad (4.28)$$

where ΔV_1 and ΔV_2 are the difference between the smooth and rough pipe flow speeds due to θ_1 and θ_2, respectively.

Since ΔV_1 and ΔV_2 are functions are two random variables θ_1 and θ_2, to measure the statistical errors, the corresponding probability density functions are calculated using the method presented in Appendices A and B.

4.3.2. Doppler Effect Ultrasonic Flowmeter

A schematic of the Doppler ultrasonic flowmeter is illustrated in Fig. 4.8. Transducer A emits a narrow beam of sound into flow at an angle γ to the flow axis. Interaction with some bubbles or particles in the flow within the incident beam results in isotropic

scattering of the incident beam. Transducer B receives the scattered beam which undergoes a frequency shift f_d proportional to flow velocity v according to the well-known Doppler equation [67],

$$V_S = \frac{f_d C_f}{2 f_e \cos\gamma} \tag{4.29}$$

where V_S is the flow speed in smooth surface pipe, C_f is the speed of sound in the flow, and f_e is the emitted frequency by transducer A.

- *Calculation of the flow velocity error due to deviation of ultrasound beams*

As the ultrasound beams are bended due to the roughness of surface, the angle between emitted beam and the flow axis γ is changed. This makes error in the calculated velocity given by Eq. (4.29). As seen in Fig. 4.7, in the case of surface roughness, the angle between emitted beam and the flow axis gets deviated by θ_1 results in changing of this angle from γ to $\gamma - \theta_1$. Therefore the velocity of the flow given in Eq. (4.29) is changed to,

$$V_R = \frac{f_d C_f}{2 f_e \cos(\gamma - \theta_1)} \tag{4.30}$$

Therefore,

$$\Delta V = V_R - V_S = \frac{f_d C_f}{2 f_e}\left(\frac{1}{\cos(\gamma - \theta_1)} - \frac{1}{\cos\gamma}\right) \tag{4.31}$$

Since θ_1 is a random variable, ΔV will be also a random variable. The deviation of ΔV can be found by using the statistical analysis given in Appendices A and B.

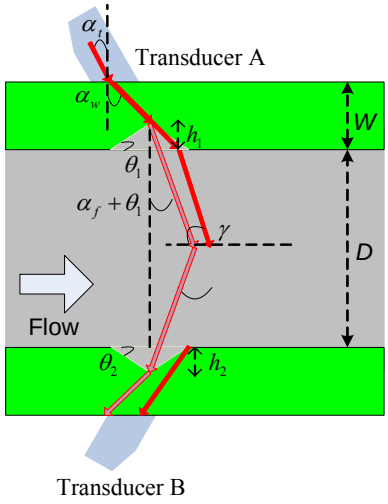

Fig. 4.8. Schematic diagram of the Doppler ultrasonic transducer.

4.4. Simulation Results

In this study, to analyze only the effect of surface roughness on the ultrasonic, we made a few assumptions and some certain numerical settings as follows,

i) The temperature distribution in the wedge is uniform so that the ultrasound beam has no deflection within the wedge.

ii) The incidence angle which is determined by the wedge is critical angle for the mode conversion of longitudinal waves into shear waves at the interface between wedge and pipe. In this study, to produce minimum beam divergence and strong shear wave in the flow, the incidence angle in wedge is set to 26˚.

iii) We assumed that the emitted beam is strong enough so that the noise caused by multiple reflections in the pipe wall and flow are eliminated.

iv) The diameter of the transducer is considered large enough to be assumed as a plane wave in Snell law.

v) The pipe diameter is considered so large compared with the wedge. Therefore the contact area of the wedge bottom with the pipe wall is an ideal line

contact. In this study, the respective wedge width and pipe diameter are set to 30 mm and 500 mm.

In this work, water and steel were considered for the flow and pipe, respectively. We plot the graphs for the beam drift and velocity variation due to deviation of ultrasonic beam with different Reynolds numbers. From Fig. 4.9 we can see that the higher Reynolds number comes with larger beam drifts in transit-time ultrasonic type. Also, it is seen that the beam drift is linearly increased with the surface roughness by around 0.8×10^{-4}. After this roughness level, this drift is substantially increased in nonlinear way.

Figs. 4.10 and 4.11 show the variation of calculated flow velocity with respect to the surface roughness with different Reynolds numbers. We see that the transit-time ultrasonic flowmeter is more affected by the surface roughness compared to the Doppler type. Also, in both cases, the Reynolds number has the same influence on the accuracy of the calculated flow velocity so that with the same roughness level, the calculated flow velocity has less accuracy for higher Reynolds number.

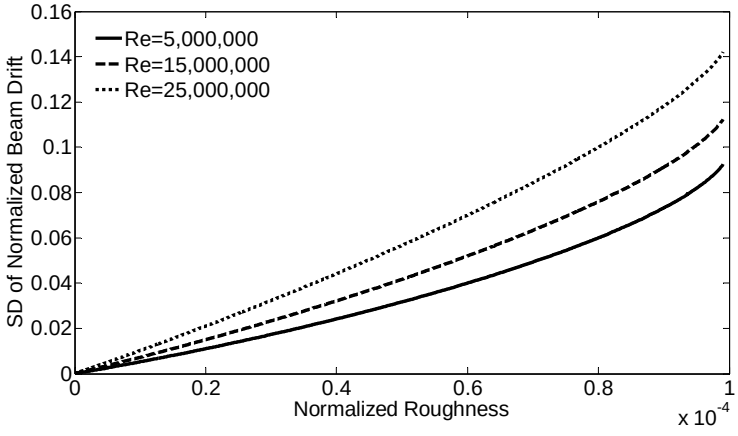

Fig. 4.9. Standard deviation of normalized beam drift in transit-time ultrasonic flowmeter.

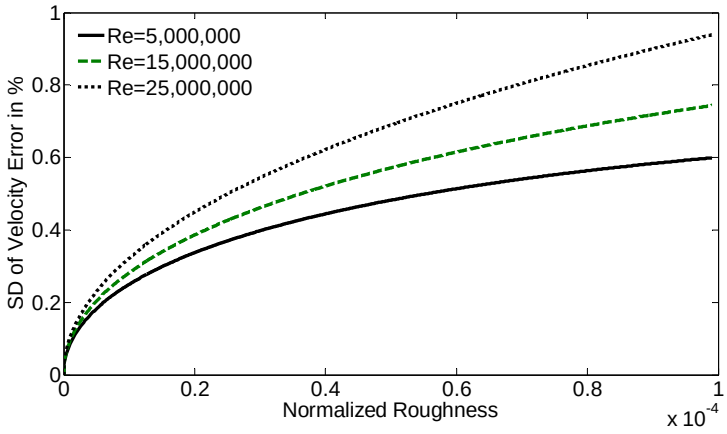

Fig. 4.10. Standard deviation of velocity error in transit-time ultrasonic flowmeter.

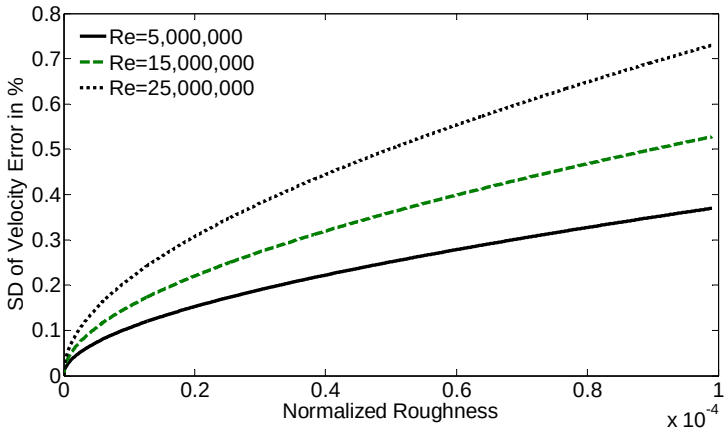

Fig. 4.11. Standard deviation of velocity error in Doppler ultrasonic flowmeter.

4.5. Conclusions

In this chapter, a brief review on the ultrasonic flowmeter technologies was presented. In addition, computer simulations for the effect of surface roughness on the performance of these flowmeters were done. It was conducted that the Doppler flowmeter is less sensitive to this problem compared to the transit-time type.

CHAPTER 5

FUTURE DIRECTON ISSUES

The future direction issues are summarized as,

- Changing the physical setting of the flow measurement system such as the pipe diameter and the thermocouple spacing to examine the rangeablity and repeatability of the flowmeter.
- Adding more thermocouples to take advantage of multiple sensing.
- Applying this flowmeter to other corrosive environments such as underground hydrocarbon reservoirs and storages.
- Applying the proposed signal processing methods to the cross-correlation ultrasonic flowmeter

APPENDIX A

A Method for the Probability Density Function (pdf) Calculation

Let *u* and *v* denote random variables with known pdf $f_U(u)$ and $f_V(v)$, respectively. Let $y = g(u,v)$ be the real-valued functions of the real variables *u* and *v*. For the sake of simplicity and without loss of generality, it is assumed that $f_U(u)$ and $f_V(v)$ are uniform distributions with following pdfs,

$$f_U(u) = \begin{cases} \frac{1}{a} & 0 < u < a \\ 0 & Otherwise \end{cases} \quad (A.1)$$

$$f_V(v) = \begin{cases} \frac{1}{b} & 0 < v < b \\ 0 & Otherwise \end{cases} \quad (A.2)$$

To obtain the pdf of $g(u,v)$ the following steps are accomplished,

Step1: *Generating numbers on intervals (0, a) and (0, b) based on the pdfs* $f_U(u)$ *and* $f_V(v)$.

In this step, for each random variable u and *v*, *N* numbers are generated. The sample interval is determined by the corresponding pdfs of the random variables. Here, for the uniform distribution over interval (0, *a*) the sample interval is fixed and equal to $\frac{a}{N}$.

Step 2: Mapping the numbers generated in step 1 to a real surface using function $y = g(u,v)$

Step 3: Mapping each point of the surface obtained in step to a line and arranging them in ascending order such that the respective minimum and maximum points of this surface go to the starting and ending point of this line.

Step 4: Splitting the line obtained in step 2 into *M* equal small elements and counting the number of points that fall on each element. Note that *M* must be chosen large enough such that on all elements at least one point falls.

If m_i is the middle point of element *i*, and n_i is the number of points that falls on this element, then the pdf of $g(u,v)$ at m_i can be approximated by,

$$f_Y(m_i) \cong \frac{M}{N}\frac{n_i}{y_{\max}} \tag{A.3}$$

Proof:

Assume that *s* and *t* are boundary points on the element *i*,

$$\Pr(s \le y \le t) = \frac{n_i}{N} \tag{A.4}$$

Also we have,

$$\Pr(s \le y \le t) = \int_s^t f_Y(y)dy \cong f_Y(m_i)\int_s^t dy = f_Y(m_i)\frac{y_{\max}}{M} \tag{A.5}$$

Combining Eq (27) and (28) gives the proof.

APPENDIX B

Calculation of the pdf of beam drifts

As random variables Δl_1 and Δl_2 are independent, we can calculate them separately. To do so, the following method is applied.

To obtain the probability density function of Δl, that is sum of random variables Δl_1 and Δl_2, one may have,

$$f_{\Delta L}(\Delta l) = \frac{d}{d\Delta l}\left(\int_{-\infty}^{+\infty}\left[\int_{-\infty}^{\Delta l-\Delta l_1} f_{\Delta L_1,\Delta L_2}(\Delta l_1,\Delta l_2)d\Delta l_2\right]\right)d\Delta l_1 \tag{B.1}$$

where $f_{\Delta L_1,\Delta L_2}(\Delta l_1,\Delta l_2)$ is the joint probability density function of random variables Δl_1 and Δl_2, that is find by:

$$f_{\Delta L_1,\Delta L_2}(\Delta l_1,\Delta l_2) = f_{\Delta L_1}(\Delta l_1) f_{\Delta L_2}(\Delta l_2) \tag{B.2}$$

where $f_{\Delta L_1}(\Delta l_1)$ and $f_{\Delta L_2}(\Delta l_2)$ are calculated using the method in Appendix A.

REFERENCES

[1]. www.omega.com, *Flow & Level Measurement, Trans. in Measurement and Control,* vol. 4.

[2] http://www.habmigern2003.info

[3] www.gfsignet.com

[4] T.H.J.J. Hagen van der and J. Voet van der ,"Interpretation of velocities determined by noise analysis," *Progress in Nuclear Energy*, vol.21, pp. 565-573, (1988).

[5] G. Por, M. Berta, M. Csuvar, "Measurement of the coolant flow rate using correlation of temperature fluctuations," *Progress in Nuclear Energy,* Vol. 43, no. 1- 4 , pp. 281-288, (2003).

[6] R.C. Baker, *Flow Measurement Handbook, Industrial Designs, Operating Principles, Performance, and Applications*, Cambridge University Press, (2000).

[7] Wikipedia. *Piezoelectric sensor*. cited; Available from: http://en.wikipedia.org/wiki/Piezoelectric_sensor.

[8] C. Crowe, M. Sommerfeld, and Y. Tsuji, *Multiphase Flows with Doplets and particles*, CRC Press LLC, (1998).

[9] V. Hans, et al., "Vortex shedding flowmeters and ultrasound detection: signal processing and influence of bluff body geometry," *Flow Measurement and Instrumentation*, vol. 9, no.2, pp. 79-82. (1998).

[10] A. Calogirou, J. Boekhoven, and R.A.W.M. Henkes, "Effect of wall roughness changes on ultrasonic gas flowmeters," *Flow Measurement and Instrumentation*, vol. 12, no.3, pp. 219-229, (2001).

[11] N. I. Loginov, *The Experience of Development and Application of Electromagnetic Flowmeters for Lead-Bismuth*, in *Heavy Liquid metal Coolants in Nuclear Technology,* Obninsk, Russia, (1998).

[12] T. Povey and P. F. Beard, "A novel experimental technique for accurate mass flow rate measurement," *Flow Measurement and Instrumentation,* vol. 19, no. 5, pp. 251-259, (2008).

[13] Y. Inoue, H. Kikura, H. Murakawa, M. Aritomi, and M. Mori, "A study of ultrasonic propagation for ultrasonic flow rate measurement," *Flow Measurement and Instrumentation,* vol. 19, no. 3-4, pp. 223-332, (2008).

[14] B.G. Liptak, *Flow Measurement*. Chilton Book Company, (1993).

[15] P.G. Bentley and D.G. Dawson, "Fluid flow measurement by temperature fluctuations," *Trans. Society of Instrument Technology*, vol. 18, pp. 183-193, 1966.

[16] http://www.maxiflo.co.kr/English/Technology/flowmetertypes.htm.

[17] S.A. Abeysekera and M.S. Beck, "Cross-correlation technique applied to pulsating flow measurement," *Measurement and Control*, vol. 3, pp. T109-T112, (1970).

[18] X. Sun, Z. Dai, Y. Weng, and J. Xu, "Experimental study on flow rate measurement by using cross-correlation of temperature fluctuations," vol. 334, *in Proc. of the ASME Heat Transfer Division,* vol. 3, 1996, *International Mechanical Engineering Congress and Exposition (IMECE),* Nov. 17-22, pp. 193-199, (1996).

[19] X. Sun, Z. Dai, and J. Xu, "A prototype of on-line digital flow meter based on cross-correlation principle, " *in Proc. the Fifth International Topical Meeting on Nuclear Thermal Hydraulics, Operations and Safety (NURETH-5),* Apr. 14-18, Beijing, China, pp. FF2-1−FF2-5, (1997).

[20] http://www.isa.org/~powid/powid_99/0194.pdf.

[21]G. V. Arkadov, O. V. Ovcharov, v. I. Pavelko, A. I. Usanov, P. Liptak, and R. Slovak, "Measurement of the coolant flow rate through a VVER-440 fuel channel on the basis of fluctuations of direct-charge sensor signals," *Atomic Energy,* vol. 91, no. 3, pp. 695-703, (2001).

[22] S. Ibrahiml and R. G. Green, "Velocity measurement using optical sensors," *in Proc. IEEE ICSE2002,* Penang, Malaysia, (2002).

[23]W. Q. Yang and M. S. Beck, "An intelligent cross correlator for pipeline flow velocity measurement," *Flow Measurement and Instrumentation*, vol. 8, no. 2, pp. 77-84, (1997).

[24] P. Benes and K. Zehnula, "New design of the two-phase flow meters," *Sensors and Actuators,* vol. 86, pp. 220-225, (2000).

[25]H. Knapp and G. C. Carter, "The generalized correlation method for estimation of time delay," *IEEE Trans. Acoust., Speech, Signal Process*, vol. 24, no. 4, pp. 320–327, (1976).

[26] J. N. Ash and R. L. Moses, "Acoustic time delay estimation and sensor network self-localization: Experimental results," *Journal of Acoustical Society of America*, vol. 188, no. 2, pp. 841–850,(2005).

[27] S. Hirata and T. Karagiri, "Cross-correlation by single-bit signal processing for ultrasonic distance measurement," *IEICE Tans. Fundamentals,* vol. E91–A, no. 4, pp. 1031-1037, (2008).

[28] M. S. Beck and A. Plaskowski, *Cross correlation Flowmeters, Their design and Application.* Adam Hilger, Bristol, (1987).

[29] H. A. Rowe, *Signals and Noise in Communication Systems.* New York: Van Nostrand-Reinhold, (1965).

[30] A. J. Weiss and E. Weinstein, "Fundamental limitations in passive time delay estimation, part I: Narrow-band systems," *IEEE Trans. Acoust., Speech, Signal Process.*, vol. 31, no. 2, pp. 472–485, (1983).

[31] L. M. Jiji, *Heat Convection*, Springer, (2006).

[32] B. Edgar Jr. Bowles, and A. G. Terrence "Flow calibration laboratory performance – What should your expectations be?," *Flow Control Magazine*, Mar./Apr., (2001).

[33] *Handbook of Measuring System Design*, John Wiley & Sons, Ltd, (2005).

[34] www.aplmf.org .

[35]. M. J. Shafer, and F. W. Ruegg, "Liquid-flowmeter calibration techniques, *Trans. of the ASME,* October, pp. 1369-1375, (1958).

[36] H. W. Coleman, and W. G. Steele, "*Experimentation and uncertainty analysis for engineers*," John Wiley & Sons, Inc., New York, (1989).

[37] J.T. Park, K.A. Behring II, and P.J. Krueger, "Metering research facility program: Review of field meter provers," *GRI Topical Report* , no. GRI-95/0209, GRI Contract no. 5086-271-2197, Gas Research Institute, Chicago, Illinois, Dec. (1995).

[38] Gallager and E. James, "Flowmeter calibration technology for natural gas," *Committee on Petroleum Measurement Spring Meeting, American Petroleum Institute*, New Orleans, LA, Mar. 29-Apr. 2, (1999).

[39] R. S. Figliola and D. E. Beasley, "*Theory and design for mechanical measurements,"* Second Edition, Wiley and Sons, New York: (396-401, 445-449), (1995).

[40] J. Yoder, "Flowmeter calibration: How, why, and where," *Control for the Process Industries,* Aug. (2000).

[41] General electric BWR thermal analysis basis (GETAB): Data, correlation and design application, *General Electric*. NEDO-10958-A. (1977).

[42] Calibration for beaver valley unit 2 LEFM checkplus system. ML129. Caldon, Inc.

[43] N. H. Sato, Y. Terao, M. Takamoto, "A new calibration facility for water flow rate at high Reynolds number," *Flow Measurement and Instrumentation,* vol. 20, no. 1, pp. 38-47, March (2009).

[44] K. Okamoto and H. Kikura, "NPP power uprates using ultrasonic flowmeter. *J At Energy Soc Japan*; vol. 49, no.1 pp. 39-44, (2007).

[45] P. D. Lysaka, D. M. Jenkinsa, D. E. Caponea and W. L. Brownb, "Analytical model of an ultrasonic cross-correlation flow meter," part 2: Application, *Flow Measurement and Instrumentation*, vol. 19, no. 1, pp. 41-46, (2008).

[46] S. Frank, C. Heilmann and H. E. Siekmann, "Point-velocity methods for flow-rate measurements in asymmetric pipe flow," *Flow Measurement and Instrumentation,* vol.7, no.3-4, pp. 201-209, (1996).

[47] J. C. Jung *et al.*, "Nonlinear correlation model for estimation of flow profile correction factor of ultrasonic flow meter in nuclear power plants," in *Proc. ICAPP'03*, May (2003).

[48] M.L. Sanderson and H. Yeung, "Guidelines for the use of ultrasonic non-invasive metering techniques," *Flow Measurement and Instrumentation*, vol. 13, pp. 125–142, (2002).

[49] K. Kikuchi , Y. Takeda, H. Obayashi, M. Tezuka, and H. Sato, "Measurement of LBE flow velocity profile by UDVP," *Journal of Nuclear Materials* , vol. 356, pp. 273–279, (2006).

[50] K. Tezukaa, M. Moria, T. Suzukia, and T. Kanamineb, "Ultrasonic pulse-Doppler flow meter application for hydraulic power plants," *Flow Measurement and Instrumentation*, vol.19, pp. 155–162, (2008).

[51] Doorman F. NAM, *private communication*, (1999).

[52] de Boer G. Instromet, *private communication*, (1999).

[53] C.-K. Jena,*, J.-G. Legouxa, L. Parentb, "Experimental evaluation of clad metallic buffer rods for high temperature ultrasonic measurements," *NDT&E International*, vol. 33, pp. 145–153, (2000).

[54] Y. Takeda, "Measurement of velocity profile of mercury flow by ultrasound Doppler shift method," *Nuclear Technology* , vol. 79, pp. 120–124, (1987).

[55] Y. Inouea, H. Kikuraa, H. Murakawaa, M. Aritomia, and M. Morib, "A study of ultrasonic propagation for ultrasonic flow rate measurement," *Flow Measurement and Instrumentation* , vol.19, pp. 223–232 ,(2008).

[56] Y.Takeda, "Velocity profile measurement by ultrasonic Doppler method," *Experimental Thermal Fluid Science*, vol. 10, pp. 444–453, (1995).

[57] M. Mori, Y. Takeda, T. Taishi, N. Furuichi, M. Aritomi, and H. Kikura, "Development of a novel flow metering system using ultrasonic velocity profile measurement," *Experiments in Fluids* , vol. 32, pp. 153–160, (2002).

[58] S. Wada, H. Kikura, Y. Koike, M. Aritomi, M. Mori, and Y. Takeda, "Development of pulse ultrasonic Doppler methods for flow rate measurement in power plant," *Journal of Nuclear Science and Technology*, vol. 41, pp. 339–346, (2004).

[59] K. Tezuka, M. mori, T. Suzuki, M. Aritomi, H. Kikura, and Y. Takeda, "Assessment of effects of pipe surface roughness and pipe elbows on the accuracy of meter factors using the ultrasonic pulse Doppler method," *Journal of Nuclear Science and Technology,* vol. 45, no. 4, pp. 304–312 ,(2008).

[60] M. Mori et al., ''Industrial application experiences of new type of flowmetering system based on ultrasonic-Doppler flow velocity profile measurement,'' *Proc. of 3rd ISUD*, pp. 115–122, (2002).

[61] H. Kikura et al., ''Development of plus ultrasonic Doppler method for flow rate measurement of power plant,'' *Proc. of ICONE 10-22574* [CD-ROM] (2002).

[62] M. Mori et al., ''Development of new type of flowmetering system by visualizing flow profile using ultrasonic-Doppler profile velocimetry,'' *Proc. of 4th WCIPT,* pp. 516–521, (2005).

[63] H.J. Dane and R. Wilsack, "Upstream pipe wall roughness influence on ultrasonic flow measurement*," North Sea Flow Measurement Workshop*, Oslo, Norway, (1999).

[64] CF Colebrook, "Turbulent flow in pipes with particular reference to the transition region between the smooth and rough pipe laws," J Inst Civil Engrs, pp. 133–56, (1939)

[65] KJ Zanker, "The effect of Reynolds number, wall roughness and profile asymmetry on single and multi-path ultrasonic meters," *North Sea Flow Measurement Workshop,* (1999).

[66] M. V. Zagarola et al., ‘‘Mean-flow scaling of turbulent pipe flow,’’ *Journal of Fluid Mechanic,* vol. 373, pp. 33–79, (1998).

[67] D. M. Dipietro and J. D. Meindl,“ Optimal system design for an implantable CW Doppler ultrasonic flowmeter,” *IEEE Trans. on Biomedical Engineering*, vol. bme-25, no. 3, (1978).

VITA

Graduate College
University of Nevada, Las Vegas

Taleb Maozzeni

Degrees:

Bachelor of Science, Electrical Engineering, 1999
Shiraz University, Iran

Master of Science, Automation and Instrumentation Engineering, 2005
Petroleum University of Technology, Iran

Publications:

Journal Papers

1. T. Moazzeni, J. Ma, Y. Jiang, and Ning Li, "Flow Rate Measurement in a High Temperature, Radioactive, and Corrosive Environment," Accepted to publish in *IEEE Transactions on Measurement and Instrumentation*, Jan. 2010.

2. T. Moazzeni, J. Ma, Y. Jiang, and Ning Li, "Calibration of Correlated Thermal Signals based Flowmeter ," to be submitted.

3. T. Moazzeni, Y. Jiang, and H. Selvarag, "A Novel Multi-Exponential Function-based Companding Algorithm for Uniform Signal Compression over Channels with Limited Dynamic Range," to be submitted.

Conference Papers

4. T. Moazzeni,Y. Jiang, J. Ma, and N. Li, "Algorithms for the Measurement of Liquid Metal Coolant Flow Velocity with Correlated Thermal Signals," *In Proc. of 9th IEEE International Conference on Signal Processing*, pp. 2702 – 2707, Oct. 2008.

5. J. M. Karthikeya Udayagiri.V.R, T. Moazzeni, Y.Jiang, and B. Das, "Detection Algorithms for the Nano Nose," *In Proc. of 19th IEEE International Conference on Systems Engineering*, pp. 399 – 404, Aug. 2008.

6- T. Moazzeni, "A Wireless Propagation Channel Model with Meteorological Quantities Using Neural Networks," *In Proc. of 3rd IEEE Consumer Communications and Networking Conference*, pp.1307 – 1309, Jan. 2006.

7. T. Moazzeni, "TOA Estimation with Meteorological Conditions Using Neural Networks", *IEEE Asia Pacific Conference on Applied Electromagnetics*," Hyatt Regency, Johor Bahru, Malaysia, Dec. 2005.

8. T. Moazzeni, A. Fatehi, and B. Araabi, "Simulation of the Steam Generator of a Gas Refinery using Neural Networks", *IEEE Canadian Conference On Electrical and Computer Engineering, Saskatoon, Canada*, May 2005.

9. T. Moazzeni, "Neural Modeling of Boiler Evaporation System of a Gas Refinery with Nonmeasurable State Variables", *IEEE International Conference On Engineering of Intelligent Systems*, Islamabad, Jan. 2006.

Dissertation Title: Flow Rate Measurement in a High Temperature, Radioactive, and Corrosive Environment

Dissertation Committee:

Chairperson, Yingtao Jinag, Ph. D.
Committee Member, Jian Ma, Ph. D.
Committee Member, Biswajit Das, Ph. D.
Committee Member, Mei Yang, Ph. D.
Graduate Faculty Representative, Hui Zhao, Ph. D.